

1539

SCP  
5-1765

**SANDIA REPORT** SAND85-0855 • Unlimited Release • UC-70

Printed March 1986

NNA.870721.0004

**Nevada Nuclear Waste Storage Investigations Project**

**Fluid Flow in a Fractured  
Rock Mass**

SAIC/T&MSS

JUL 21 1987

CCF RECEIVED

E. A. Klavetter, R. R. Peters

Prepared by  
Sandia National Laboratories  
Albuquerque, New Mexico 87185 and Livermore, California 94550  
for the United States Department of Energy  
under Contract DE-AC04-76DP00789

HYDROLOGY DOCUMENT NUMBER 433

"Prepared by Nevada Nuclear Waste Storage Investigations (NNWSI) Project participants as part of the Civilian Radioactive Waste Management Program (CRWM). The NNWSI Project is managed by the Waste Management Project Office (WMPO) of the U. S. Department of Energy, Nevada Operations Office (DOE/NV). NNWSI Project work is sponsored by the Office of Geologic Repositories (OGR) of the DOE Office of Civilian Radioactive Waste Management (OCRWM)."

Issued by Sandia National Laboratories, operated for the United States Department of Energy by Sandia Corporation.

**NOTICE:** This report was prepared as an account of work sponsored by an agency of the United States Government. Neither the United States Government nor any agency thereof, nor any of their employees, nor any of their contractors, subcontractors, or their employees, makes any warranty, express or implied, or assumes any legal liability or responsibility for the accuracy, completeness, or usefulness of any information, apparatus, product, or process disclosed, or represents that its use would not infringe privately owned rights. Reference herein to any specific commercial product, process, or service by trade name, trademark, manufacturer, or otherwise, does not necessarily constitute or imply its endorsement, recommendation, or favoring by the United States Government, any agency thereof or any of their contractors or subcontractors. The views and opinions expressed herein do not necessarily state or reflect those of the United States Government, any agency thereof or any of their contractors or subcontractors.

Printed in the United States of America  
Available from  
National Technical Information Service  
U.S. Department of Commerce  
5285 Port Royal Road  
Springfield, VA 22161

NTIS price codes  
Printed copy: A04  
Microfiche copy: A01

FLUID FLOW IN A FRACTURED ROCK MASS\*

by

E. A. Klavetter and R. R. Peters  
Nevada Nuclear Waste Storage Investigations Project Department  
Sandia National Laboratories  
Albuquerque, New Mexico 87185

ABSTRACT

The geological formations in the unsaturated zone underlying Yucca Mountain, on and adjacent to the Nevada Test Site, are being evaluated by the Nevada Nuclear Waste Storage Investigations project. The formations are being considered as host media for a radioactive-waste repository. They are composed of tuffaceous materials, sometimes highly fractured, whose hydrologic properties must be evaluated to estimate the rate at which radionuclides could migrate to the accessible environment. Hydrologic flow models used for postclosure performance assessment of the prospective repository must take into account the potential for water movement in both the rock matrix and the fractures. Calculations using models that explicitly account for the effects of individual fractures are not feasible, because of the extremely large number of fractures contained in a site-scale problem and the difficulties in characterizing and modeling the fracture geometries.

Two approaches were used to develop a continuum model to evaluate water movement in a fractured rock mass. Both approaches assume that the pressure heads in the fractures and the matrix are identical along a line perpendicular to flow. The first approach uses this assumption and separate equations for flow in the fractures and in the matrix to derive both a single flow equation for an equivalent, porous medium and mathematical expressions for the unsaturated, hydrologic properties in this flow equation. The second approach assumes a fluid continuity equation for a porous medium. Information on the physical structure of the rock mass, along with theoretical considerations from capillary theory, is used to derive the mathematical expressions for the rock-mass unsaturated hydrologic properties. Both approaches lead to a single flow equation for a fractured rock mass.

The two approaches were used to calculate unsaturated hydrologic properties, i.e., relative permeability and saturation as a function of pressure head, for several types of tuff underlying Yucca Mountain, using the best available hydrologic data for the matrix and the fractures. Comparisons of properties calculated by both approaches were found to yield qualitatively and quantitatively similar results.

---

\* This work, performed at Sandia National Laboratories, was supported by the U.S. Department of Energy under contract number DE-AC02-76DP00789.

TABLE OF CONTENTS

	<u>Page</u>
ABSTRACT . . . . .	i
LIST OF FIGURES . . . . .	iii
LIST OF TABLES . . . . .	iv
NOTATION . . . . .	v
INTRODUCTION . . . . .	1
HYDROLOGIC MODELS . . . . .	9
Macroscopic Derivation of the Equation for Water Flow . . . . .	12
Microscopic Derivation of the Flow Equation . . . . .	32
SUMMARY . . . . .	44
REFERENCES . . . . .	45

LIST OF FIGURES

<u>NO.</u>	<u>TITLE</u>	<u>Page</u>
1	Location of Yucca Mountain, Nevada . . . . . Outline indicates preliminary repository boundary. Cross section in Fig. 3 is along line L-L'.	2
2	Comparison of the formal geologic and functional stratigraphy in Drill Hole USW G-4 . . . . .	3
3	Conceptual model of flow at Yucca Mountain . . . . . Cross section is along line L-L' in Fig. 1	5
4	Conceptual model for flow in a fracture at increasing levels of saturation . . . . .	7
5	Saturation curve for sample G4-6 taken from Unit TSw2 . . . . .	19
6	Representative matrix-saturation curves for the unsaturated-zone, hydrologic units . . . . .	19
7	Capacitance coefficients for Unit PTn . . . . .	25
8	Capacitance coefficients for Unit TSw2 . . . . .	25
9	Capacitance coefficients for Unit CHnz . . . . .	26
10	Conductivity curve for Unit PTn . . . . .	28
11	Conductivity curve for Unit TSw2 . . . . .	28
12	Conductivity curve for Unit CHnz . . . . .	29
13	Incremental volume versus pore diameter for sample G4-6 from Unit TSw2 . . . . .	35
14	Hydraulic conductivity comparison for material representative of Unit TSw2 . . . . .	40
15	Hydraulic conductivity comparison for material representative of Unit TSw3 . . . . .	41
16	Hydraulic conductivity comparison for material representative of Unit CHnz . . . . .	42

LIST OF TABLES

<u>NO.</u>	<u>TITLE</u>	<u>Page</u>
1	Unsaturated zone, hydrologic unit properties . . . . .	21
2	Coefficients for tortuosity, exponential distribution function (Eq. 22) . . . . .	43

## NOTATION

- A - fitting parameter in Eq. 22  
B - fitting parameter in Eq. 22  
b - fracture aperture  
C - fitting parameter in Eq. 22  
E - modulus of deformation in Eq. 9  
f(b) - frequency at fracture aperture b  
g - acceleration due to gravity  
K - hydraulic conductivity  
n - porosity  
P - Mercury intrusion pressure in Eq. 20  
 $\bar{q}$  - specific discharge  
r - pore radius  
S - saturation  
t - time  
 $\bar{V}$  - deformation velocity of the media  
v(r) - incremental volume fracture at pore radius r  
z - depth or elevation

### Greek Symbols

- $\alpha$  - fitting parameter in Eq. 7  
 $\alpha_{\text{bulk}}$  - coefficient of consolidation  
 $\beta$  - fitting parameter in Eq. 7  
 $\beta_w$  - water compressibility  
 $\Gamma$  - term describing mass transfer between matrix and fractures  
 $\gamma$  - surface tension

## NOTATION CONT'D

- $\xi$  - mean in lognormal distribution (Eq. 18)
- $\theta$  - volumetric water content
- $\lambda$  - fitting parameter in Eq. 7
- $\nu$  - Poisson's Ratio
- $\rho$  - density
- $\sigma$  - variance in lognormal distribution (Eq. 18)
- $\sigma'$  - stress in rock mass
- $\phi$  - contact angle
- $\chi$  - tortuosity distribution function
- $\psi$  - pressure head
- $\omega$  - mass transfer coefficient in Eq. 4

## Subscripts

- b** - bulk, referring to a rock mass property
- bulk** - pertaining to the total rock mass
- c** - composite; combining both matrix and fractures
- f** - fracture(s)
- Hg** - mercury
- m** - matrix
- r** - residual
- rel** - relative
- s** - saturated
- tot** - total
- w** - water

## INTRODUCTION

The geological formations in the unsaturated zone at Yucca Mountain, on and adjacent to the Nevada Test Site (NTS), are currently being investigated as a possible host rock for a radioactive-waste repository; the U.S. Department of Energy (DOE) is carrying out these studies through the Nevada Nuclear Waste Storage Investigations (NNWSI) project. The Yucca Mountain site is unique among the prospective repository sites in that the proposed repository horizon lies entirely in the unsaturated zone. The purpose of this document is to discuss, in general terms, (1) the Yucca Mountain site with emphasis on characteristics that affect the hydrologic system, (2) the conceptual hydrologic model, and (3) the mathematical model of flow in the unsaturated zone. This mathematical model is the one currently being used in the NNWSI performance assessment systems code TOSPAC (Dudley et al., in preparation).

The location of Yucca Mountain is indicated in Figure 1. It lies within the physiographic Basin and Range Province which is characterized by generally linear mountain ranges and intervening valleys. Yucca Mountain is a prominent group of north-trending, fault-block ridges. The elevation of northern Yucca Mountain is approximately 1500 m. The ridge of Yucca Mountain is about 300 m above the surrounding valley floors. Yucca Mountain is made up predominantly of ash-flow and ash-fall tuffs. These tuffs may be organized into functional units that minimize the thermal, mechanical, and hydrologic property variability within each unit. Figure 2 lists the locations of the functional units at drill hole USW G-4 in terms of depth and geologic units. The functional units above the water table can be placed into one of three basic groups on the basis of properties that affect the hydrology.

1) Densely welded tuffs that are highly fractured.

These units have low saturated matrix conductivities ( $10^{-11}$  m/s or less for all but one unit) and high saturated fracture conductivities (for a unit volume of rock, the total saturated conductivity of the fracture system is probably several orders of magnitude higher than the total saturated conductivity of the matrix). The units included in this group are TCw, TSw1, TSw2, TSw3 and PPw. Unit PPw is the most porous and has the highest conductivity of any of the units in this group.

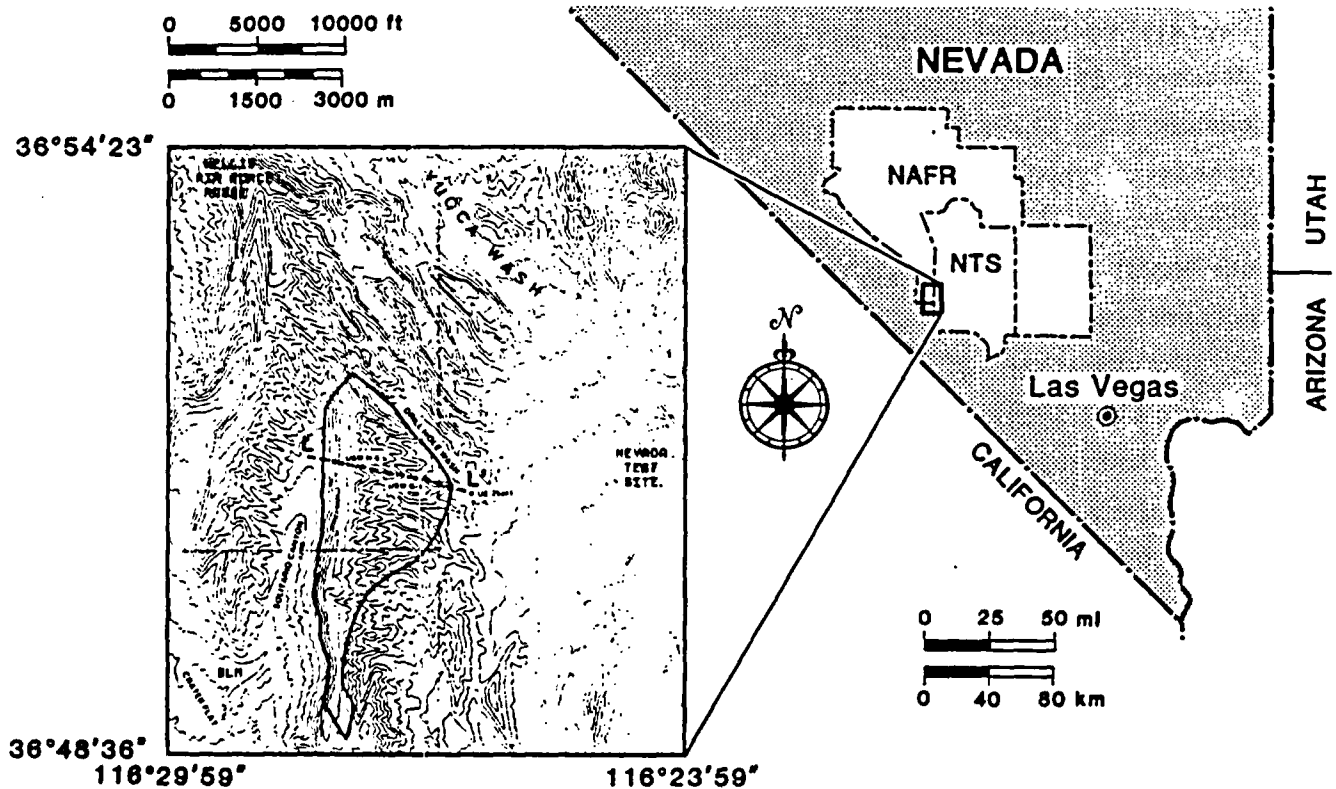
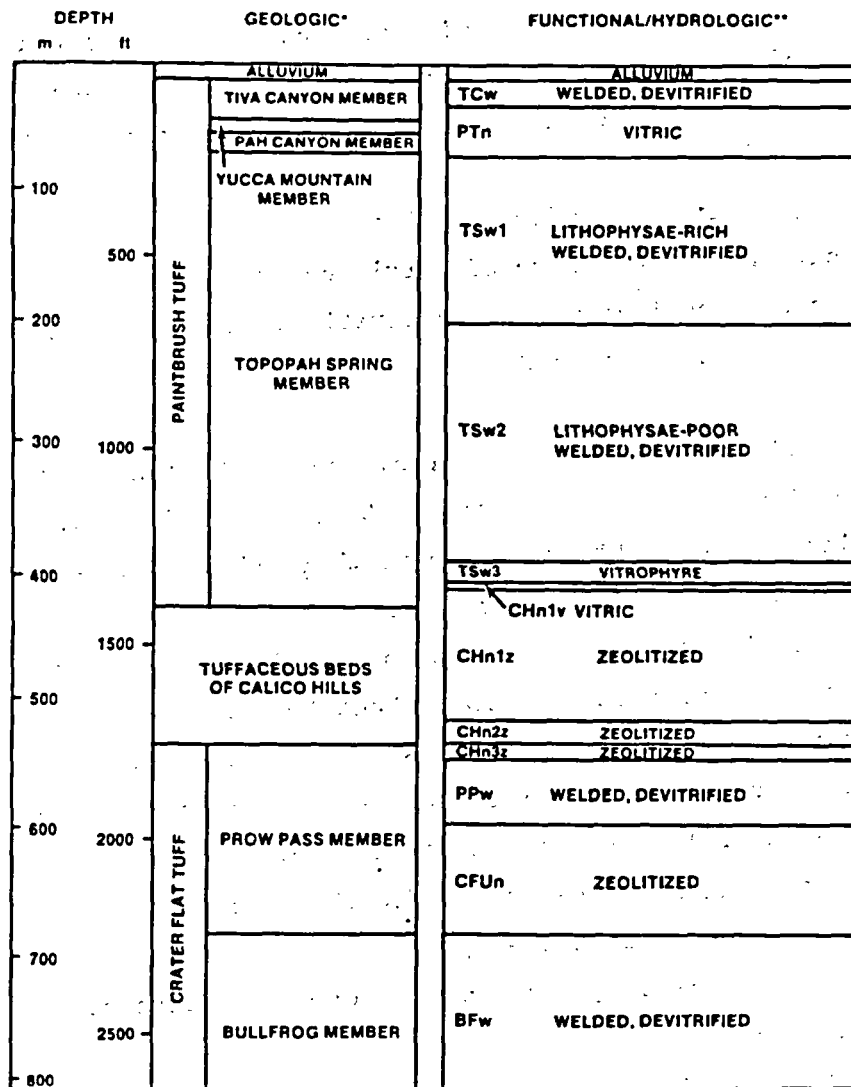


Figure 1. Location of Yucca Mountain, Nevada

Outline indicates preliminary repository boundary.  
 Cross section in Fig. 3 is along line L-L.



\*DEPTHS FROM SPENGLER ET AL. (1984)  
 \*\*DEPTHS FROM ORTIZ ET AL. (1985)

Figure 2. Comparison of the formal geologic and functional stratigraphy in Drill Hole USW G-4.

2) Nonwelded, vitric tuffs that have few fractures.

These units have high saturated matrix conductivities (in the range of  $10^{-6}$  to  $10^{-8}$  m/s) and relatively low saturated fracture conductivities. The units included in this group are PTn and CHnv.

3) Nonwelded, zeolitized tuffs that have few fractures.

These units have low saturated matrix conductivities ( $10^{-11}$  m/s or less) and low saturated fracture conductivities. The unit above the water table included in this group is CHnz.

A more complete discussion of definition of the functional units, the methods used to pick their boundaries, etc., may be found in a report by Ortiz, Williams, Nimick, Whittet, and South (1985). The report by Peters et al. (1984) shows that the units defined primarily on the basis of thermal, mechanical, and mineralogical properties are also relatively homogeneous in terms of hydrologic properties. Throughout the rest of this report, the functional units will be referred to as "hydrologic units" to emphasize the fact that these units are relatively homogeneous in terms of hydrologic properties. A general introduction to the geology of the region may be found in the Draft Environmental Assessment for the Yucca Mountain Site (DOE, 1984). Information regarding the hydrology and fracture frequency was drawn from many sources, including Scott et al. (1983), Peters et al. (1984), and Sinnock et al. (1984).

Figure 3 is an east-west cross-section through Yucca Mountain at the location (section L - L') indicated in Figure 1. It is based on information contained in the previously cited report by Ortiz. The positions of the hydrologic units are indicated along with the position of the water table and the approximate position of the repository.

A conceptual model of the the hydrologic system at Yucca Mountain is indicated schematically in Figure 3. A small fraction of the annual precipitation infiltrates the surface of the mountain. It then begins moving down through the various units. It is possible that some portion of the total flux may be diverted at interfaces between the hydrologic units due to the

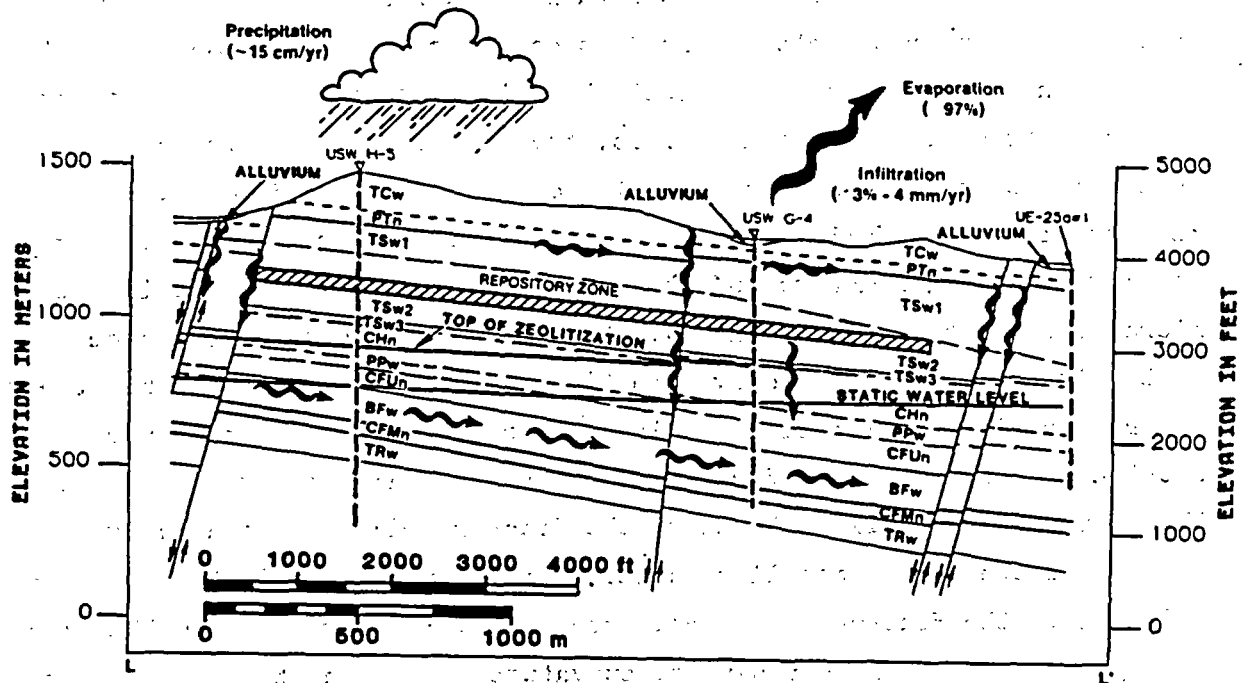


Figure 3. Conceptual model of flow at Yucca Mountain.

Cross section is along line L-L' in Fig. 1

extreme contrast in hydrologic properties between two units (e.g., PTn and TSw2). If a perched water table forms at an interface, water will be diverted down-dip. However, as a result of the extreme contrast in the conductivities of the units at the interface, it may be possible for water to be diverted down-dip without a perched water table forming at the interface between the two units. Calculations and field testing will be required to determine whether it is feasible to divert water in a situation where a perched water table does not form.

The conceptual model for flow within a fractured, porous medium used by many workers in this field is based on capillary bundle theory (e.g., Wang and Narasimhan, 1985) which states that there is a relationship between pore size and equilibrium pressure head. Thus, the saturation of a material containing pores of many different sizes is related to the equilibrium pressure head in the material. The following discussion will assume that the average fracture aperture is 25 micrometers and the matrix average pore diameter is 0.03 micrometers (Peters et al., 1984). This discussion will also assume that the system is changing very slowly with time, a condition that will be true deep underground in most locations. Figure 4 shows a plan view of a very small section of a hypothetical fracture face at four different saturations. When the matrix is partially saturated, the fracture will be essentially dry because of the higher capillary suction (tension) forces in the matrix pores adjacent to the fracture. A small amount of water may exist in the fracture in regions where a small radius of curvature can be maintained. In Figure 4a water would be contained in regions where the matrix blocks are shown as being in contact (local aperture < 0.1 micrometer) and in very thin rings around these regions. The conductivity of the fracture for water movement in the plane of the fracture is zero because these little islands of fracture water are discontinuous. However, the conductivity for water movement across the fracture is not zero; the contact regions form pipelines to transfer water from one matrix block to the next. For tuffs at Yucca Mountain, the fracture conductivity for flow across the fractures has been estimated to be high in comparison with the conductivity within the matrix (Wang and Narasimhan, 1985).

As the matrix saturation is increased, the saturation of the fracture will also increase in a highly nonlinear manner. At a higher matrix saturation (and corresponding pressure head) these islands of water may be at the point of coalescing (Figure 4b). At this pressure, the fracture conductivity in the plane of the fracture is still essentially zero while the conductivity for

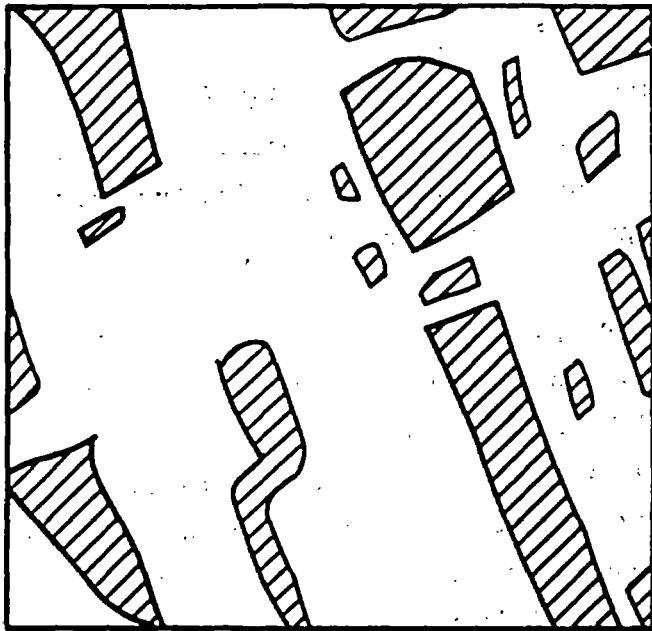


Figure 4a. Pressure head  $\approx -50$  m, fracture dry except at contacts (cross-hatch area)

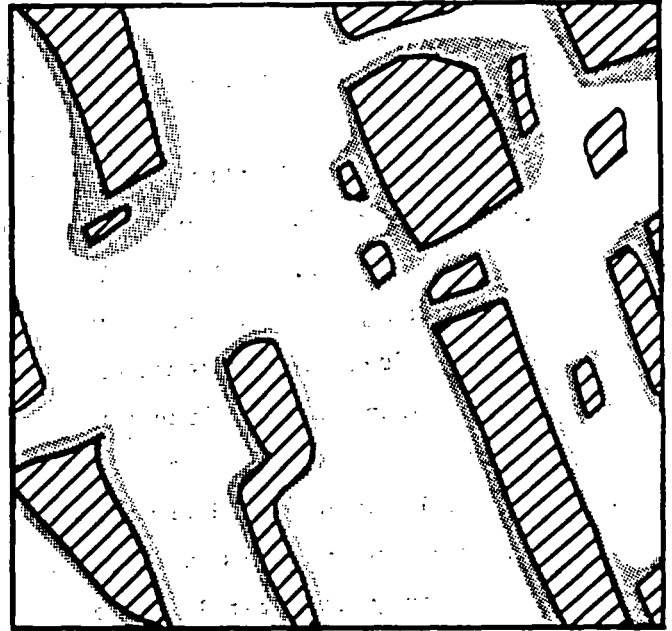


Figure 4b. Pressure head  $\approx -5$  m, rings around contacts are near coalescence

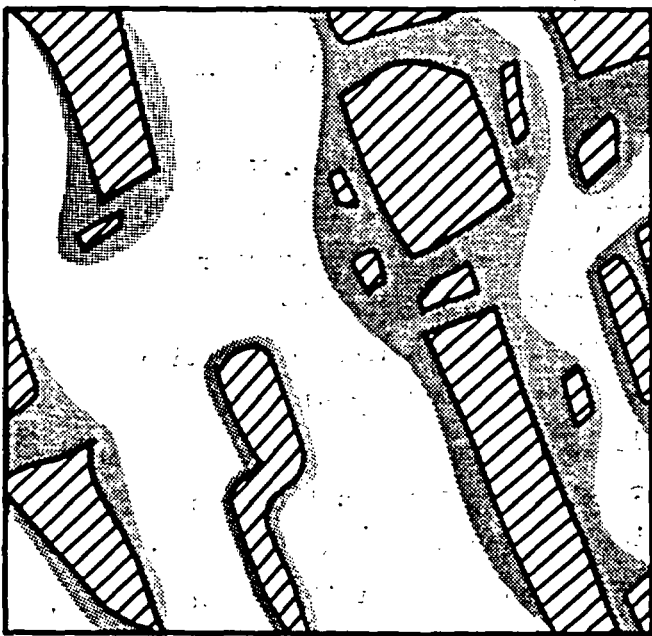


Figure 4c. Pressure  $\approx -0.5$  m, sinuous flow in fracture plane

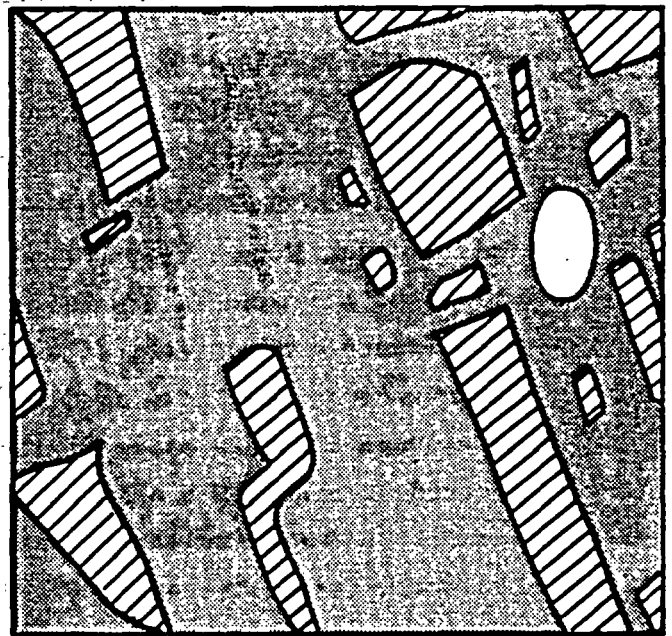


Figure 4d. Fracture near saturation, one "trapped" air bubble

Figure 4. Conceptual model for flow in a fracture at increasing levels of saturation.

water flow across the fracture has increased. At slightly higher matrix saturations (for the parameters chosen in this example the matrix saturation would be of the order of 0.99999) the islands of water in the fracture have coalesced to form sinuous channels (Figure 4c); the fracture conductivity in the plane of the fracture is now nonzero. Finally, at a pressure head approaching zero the fracture is almost completely saturated (Figure 4d).

The fracture is generally nonplanar. Thus, when there is water movement in the plane of the fracture there will be regions where there is locally high fracture flow and others where the flow is quite small. If the fracture is partially saturated the majority of flow will occur in those regions where the fracture aperture is small. Those regions where the fracture aperture is large carry no water because the aperture in this region is too large to hold any water. This concept is derived from fundamental principles of capillary theory. When the fracture is completely saturated, the situation is reversed. The majority of the flow in the fracture occurs in those regions where the fracture aperture is large, with little flow occurring where the fracture aperture is small because the flow rate is proportional to the cube of aperture (Gale, 1975).

The conceptual model of flow in fractures used in this paper is based on the previous discussion. The major points are summarized below.

- 1) The fracture conductivity for water movement across the fracture is probably much larger than the adjacent matrix conductivity. Thus, flow across the fracture is controlled by the adjacent matrix conductivity. The fracture conductivity across the fracture can be replaced by the matrix conductivity in flow calculations.
- 2) The average fracture conductivity for water movement in the plane of the fracture is a highly nonlinear function of fracture saturation or pressure head. If the flux is less than the saturated conductivity of the matrix, then the water will tend to flow only in the matrix as it moves downward. If the flux is greater than the saturated conductivity of the matrix, then the matrix will saturate, and the fractures will carry water also.

The manner in which the water flows in a hydrologic unit depends on other boundary conditions besides the flux. For example, in the capillary fringe area near the water table, the matrix is always saturated because of the capillary forces of the small pores in the matrix; thus, in this capillary fringe area some water will be in the highly conductive fractures no matter how small the downward flux is. A lengthy discussion of many different mechanisms for water movement in the unsaturated zone may be found in the report by Montazer and Wilson (1984).

#### HYDROLOGIC MODELS

The purpose of the previous section was to indicate the general setting of Yucca Mountain and a conceptual hydrologic flow model. In this section, geologic and hydrologic information is used to choose appropriate mathematical models for calculations concerning the entire Yucca Mountain site. There are currently many hydrologic codes available (e.g., NETFLO - Intera, 1982; NWFT/DVM - Campbell et al., 1981; TRUST - Reisenauer et al., 1982; and SAGUARO - Eaton et al., 1983). However, those that have tried to simulate an unsaturated, layered system where the water flow may occur in fractures as well as the matrix have had numerical-stability problems (e.g., Bixler and Eaton, in preparation). The purpose of the following sections is to review the general equations for flow in a porous media, discuss the problems associated with using the models, and discuss the alternatives available. The flow model discussed in this paper may be used by TOSPAC, a code being developed for systems studies of Yucca Mountain, and other NNWSI hydrologic codes.

The derivation of the equation for water flow in partially saturated, porous media is given in many papers (e.g., Reeves and Duguid, 1975; Freeze and Cherry, 1979; and Narasimhan, 1982). It generally begins with the expression for the conservation of fluid mass in the absence of either sources or sinks. The assumptions used in deriving the somewhat restricted equation for fluid flow are

- 1) Darcy's equation may be used to calculate the flow.
- 2) The matrix is rigid.
- 3) The flow is isothermal.

The result is Richards's equation (Richards, 1931).

$$\frac{\partial(\rho\theta)}{\partial t} = \nabla \cdot \rho[K \cdot \nabla(\psi + z)]$$

where 
$$\frac{\partial(\rho\theta)}{\partial t} = \frac{\partial(\rho n S)}{\partial t}$$

$$= \rho n \frac{\partial S}{\partial t} + n S \frac{\partial \rho}{\partial t} + \rho S \frac{\partial n}{\partial t}$$

$$\approx n \left[ \rho \frac{\partial S}{\partial t} + S \frac{\partial \rho}{\partial t} \right] = n \frac{\partial \psi}{\partial t} \left[ \rho \frac{\partial S}{\partial \psi} + S \frac{\partial \rho}{\partial \psi} \right]$$

In Eq. 1,  $\rho$  is the density of water,  $\theta$  is the water content per unit volume,  $t$  is the time,  $\bar{K}$  is the hydraulic conductivity tensor that is, in general, a function of  $\psi$ ,  $\psi$  is the pressure head,  $z$  is the elevation above an arbitrarily chosen reference plane (e.g.,  $z = 0$  at the mean sea level),  $n$  is the porosity, and  $S$  is the saturation.

The determination of some of the experimental parameters used in Eq. 1 is fairly straightforward (e.g., that of  $\rho$  and the derivative of  $\rho$  with respect to  $\psi$ ); however, the determination of values for many are difficult (e.g.,  $\bar{K}$ ). As previously discussed, some of the hydrologic units are highly fractured and, depending upon the magnitude of the flux, there may be water movement in both the fractures and the matrix. Equation 1 was derived for a porous medium with no regard for the possibility of water movement in two different "media" (i.e., fractures and matrix); the derivation contains no information concerning how the coefficients should be evaluated or even what their functional form is.

There are two alternatives for modeling the situation where water movement occurs in both the fractures and the matrix with neither flow being negligible compared with the other.

- 1) Model the fractures explicitly by zoning them into the calculational mesh as a second region that has much different properties from the properties of the matrix portion.
- 2) Rederive the flow equation (Eq. 1) for an equivalent porous medium, taking into account the fact that there are two porosity systems (the matrix porosity system and the fracture porosity system).

The option of explicitly zoning in the fractures has been used by a variety of workers. This technique is well suited for "small-scale" problems such as simulating the results of laboratory or small field-scale experiments. This technique is not suited to simulations of large site-scale problems where there may be more than  $10^{10}$  fractures in the region being simulated. Thus, option 2 must be considered for modeling site-scale problems.

The development of equations describing flow in this equivalent porous medium can be derived either from a "macroscopic" or "microscopic" point of view. A macroscopic model assumes that the fracture and matrix hydrologic properties used are statistically representative of a large volume of rock mass. To derive such a model requires a set of appropriate experimental measurements: separate tests of flow through the matrix and through the fractures. The results of these tests are combined with the assumption of a constitutive equation that describes the water movement characteristics in the system of interest. Then conductivity and saturation values as a function of pressure head are indirectly determined for both a representative sample of matrix material and a representative set of fractures without requiring any actual knowledge of the physical structure of the system. For both the matrix tests and the fracture tests, the volume of rock material tested is treated as a "black box" with the constitutive equation as the transform function and the hydrological properties as the coefficients that have been determined to relate the input and output parameters. For example, in order to indirectly determine values for the hydraulic parameters, the water continuity equation or some equivalent equation (e.g., Eq. 1) may be used as the transform function, with measured values of flow rate and pressure gradient as the input and output parameters. Testing and modeling of the the combined matrix-fracture system provide the necessary information to link the behavior of the matrix and fractures.

It is also possible to derive the hydrologic-property values for a rock mass volume more directly from a microscopic approach, using the actual physical structure of the system of interest, combined with fundamental theoretical considerations of fluid flow in pores of a specific geometry, to determine relative conductivity and saturation values as a function of pressure head. In this manner, the individual hydrologic contributions of every pore size and fracture aperture are considered, rather than inherently taking a "lump-sum" average of the entire system. These values for saturation as a function of pressure head and relative hydraulic conductivity as a function of pressure head (or saturation), which are determined independently of the flow equation in which they are to be used, can then be applied to describe the movement of fluid in a fractured, porous media.

The following sections will present both a macroscopic and a microscopic derivation of the equation for water flow in a fractured, porous medium and the evaluation of the coefficients in the flow equation. We show that the results of the two derivations are nearly identical.

Both derivations draw heavily on capillary bundle theory in their evaluation of hydrologic coefficients. A calculation of the rise in height of water in a capillary tube as a function of tube radius indicates that for tubes with a radius of the order of a few millimeters, the fluid rise, due to capillary forces, is the same as the tube radius. Thus, the limit of applicability for capillary bundle theory is of the order of millimeters. This estimate of the limit of applicability indicates the models developed in this paper are not applicable for systems containing fractures with apertures of the order of many millimeters or larger.

#### Macroscopic Derivation of the Equation For Water Flow

Many authors have discussed the dual-porosity approach to modeling fractured, porous media, including personnel in the petroleum industry (Warren and Root, 1963; Odeh, 1965; Gringarten and Ramey, 1974) and those involved in hydrogeology (Barenblatt et al., 1960; Duguid and Lee, 1973). The derivation of the equation for water flow in a fractured, porous medium draws upon the work just cited, especially that of Duguid and Lee. The general fluid continuity equations in a dual-porosity equivalent continuum can be expressed as follows.

$$\frac{\partial (\rho n_m S_m)}{\partial t} + \nabla \cdot (\rho \bar{q}_m) + \nabla \cdot (\rho S_m n_m \bar{V}) + \Gamma = 0 \quad (2)$$

$$\frac{\partial (\rho n_f S_f)}{\partial t} + \nabla \cdot (\rho \bar{q}_f) + \nabla \cdot (\rho S_f n_f \bar{V}) - \Gamma = 0 \quad (3)$$

These equations are more general than Eq. 1 because they do not have the three restrictions (Darcian flow, rigid matrix, isothermal flow) placed on Eq. 1. The subscripts "m" and "f" refer to the matrix and the fractures, respectively.  $\bar{q}$  is the water's specific discharge and  $\bar{V}$  is the deformation velocity of the medium. These equations include a term for the transfer of fluid from the fracture system to the matrix ( $\Gamma$ ). Many authors (e.g., Barenblatt, 1960) calculate the transfer of flux between the two systems as

$$\Gamma = \omega(\psi_f - \psi_m) \quad (4)$$

The value of the transfer coefficient  $\omega$  is difficult to determine experimentally, and estimates usually vary over many orders of magnitude (Barenblatt et al., 1960).

Equations 3 and 4 may be added together yielding a single equation in two unknowns  $\psi_m$  and  $\psi_f$ . Thus, we need a second equation or condition concerning the linkage between  $\psi_m$  and  $\psi_f$  to solve for the flow field in a fractured, porous medium. These two variables are, of course, equal if there is no flow through the media. It is reasonable to assume that as the flow is increased from zero these two pressure heads may begin to take on increasingly different values. Then, if the flow is held constant, it is reasonable to assume that the pressure heads in the matrix and fractures will eventually equalize. Thus, it is reasonable to assume that the magnitude of the difference in matrix pressure head and fracture pressure head in a particular hydrologic unit depends on both the magnitude and history of the flux. If the flow is large and changing rapidly in time, it is reasonable to assume this difference is significant. However, the infiltration at the Yucca Mountain site is thought to be less than 1 mm/year (DOE, 1984; Montazer and Wilson, 1984) and probably changes very slowly with time at the depth of the prospective repository and below. The calculations discussed in the following

paragraphs investigate the magnitude and history of the flux with regard to the depth to which a water pulse may penetrate a fractured system. The results of the calculations concerning the flux history are then used as input to calculations to estimate the magnitude of the difference in pressure head between the fractures and the matrix under conditions that are thought to be reasonable at Yucca Mountain.

The results of calculations using explicitly zoned fractures are useful in determining whether episodic pulses of water at the surface (e.g., pulses due to large storms) will reach the repository horizon as a sharp pulse (e.g., by moving through the fractures exclusively) or as a very slowly varying pulse (e.g., by moving through the matrix in one or more units). A slowly moving pulse may, in fact, mix with other pulses, resulting in a flux that is constant at depth with respect to time. Work specifically relevant to infiltration pulses at Yucca Mountain has been done by Travis et al. (1984) and by Martinez (in preparation). In Martinez's work the surface was completely saturated for one hour, while in Travis' work a slug of water of the order of 2 m tall was injected into a 100-micrometer fracture. Both Travis and Martinez seem to indicate that episodic pulses of water at the surface will not penetrate significant distances into Yucca Mountain if the fracture aperture is less than 100 micrometers (an approximate upper value suggested by Sinnock et al. (1984)). The water injected into the fracture moves quickly into the matrix because of two complementary effects:

- 1) At the front end of the pulse, a large pressure-head difference exists between the saturated fracture and the partially saturated matrix (this difference may be of the order of 100 m).
- 2) Because the fracture conductivity ahead of the water pulse is very low (the fracture may be near its residual saturation), flow in the fracture is retarded and the pulse diverted into the matrix. Wang and Narasimhan (1985) indicate that the fracture conductivity for flow within the plane of the fracture may be zero until the nearby matrix material is nearly saturated.

The independent calculations of Martinez and Travis indicate that the penetration distance into fractures contained in low-conductivity, densely welded tuffs similar to those that form a caprock of Yucca Mountain (unit TCw) is of the order of 10 m or less if the fracture aperture is 100 micrometers or less. Calculations by Martinez of the penetration of water into fractures in unit PTn (which is above the repository zone) show much less penetration of the pulse into unit PTn than into unit TCw because the matrix of unit PTn is much more conductive.

The velocity of water movement in the matrix is of the order of the percolation rate or the saturated conductivity (whichever is less) divided by the porosity. Thus, the maximum water velocity in the matrix is of the order of ten times the flux, a value which is probably less than several millimeters per year.

Thus, there is some indication that the water flux at depth may be a slowly varying function of time, from which it may be inferred that the difference in pressure head between fractures and matrix may be small at depth. It should be noted that episodic pulses of water may penetrate to great depth in regions near large structural features, such as fault zones, or where the fracture apertures are very large so that capillary bundle theory is not applicable. Simulations of these situations have not, to the authors' knowledge, been completed, and there is only informed opinion on this last subject.

Wang and Narasimhan (1985) have simulated the drainage of a fractured, welded-tuff cube of approximately 1.5 cubic meters. This simulation gives an idea of the difference between the fracture and matrix pressure heads under conditions where the flux is a slowly varying function of time. The matrix saturation curve was based on psychrometer test results (Peters et al., 1984) with matrix desaturation occurring over the pressure head range of -100 m to -10,000 m. The matrix saturation curve used is very similar to that shown in Figure 5, which is taken from Peters et al., 1984. The cube has two orthogonal vertical fracture sets and one horizontal set that divide the simulation region up into 75 blocks (5 wide \* 5 deep \* 3 blocks high). The fracture properties and spacings were chosen to be representative of those found in a welded tuff unit at Yucca Mountain. The fracture saturation curve was developed from physical and statistical considerations with the fractures desaturating over the pressure head range of 0.0 to -0.1 m which, according to

Figure 5, is in the region where the matrix saturation deviates very little from 1.00.

The cube was initially saturated. A step change in the lower boundary's pressure head to -112 m initiated the simulation. A pressure head of -112 m in the matrix block corresponds to a saturation of 80%. Throughout the simulation the pressure head at a point in the middle of the center block was identical to the pressure head at a point in the adjacent fracture that had the same elevation as the first point. The pressure head in both the fractures and the matrix blocks varied only in the vertical direction, which was the direction of flow.

The pressure heads in the matrix and the fractures were identical because of the contrast in their saturation curves. According to Figure 5, over the pressure-head range where the fractures were desaturating (0.0 to -0.1 m of pressure head), the matrix maintained essentially constant saturation ( $S \sim 1.0$ ), and over the pressure head range where the matrix was desaturating the fractures were at nearly constant saturation (the fracture residual saturation). Therefore, during the time period when the fractures were draining, only a very small amount of water was required to drain from the matrix to maintain pressure equilibrium with the fractures. After the fractures were drained, their pressure head matched that of the matrix, because only minuscule amounts of water had to be drained from the fractures so that the pressure head in the fractures matched that of the matrix. In the problem of saturating the block slowly, the results would be identical to the drainage problem. These results indicate that the contrast in fracture and matrix properties, under conditions of slowly varying flux (either decreasing or increasing flux), constrains the pressure head in the fractures and the matrix to be nearly identical.

In summary, calculations by Travis and by Martinez indicate that periodic injections of water into the surface above the main body of the repository region are not likely to penetrate the fractures to great depth and so the flux at depth is a slowly varying function. Calculations by Wang and Narasimhan indicate that in a drainage situation (or probably its equivalent, slow saturation) the fractures and matrix, along a direction perpendicular to

flow, have nearly identical pressure heads. Thus, except near the surface (where the fracture aperture is large) and near large-scale features (e.g., fault zones), it is reasonable to assume that the pressure head in the fracture system equals that in the matrix.

Summing equations and setting  $\psi_m$  equal to  $\psi_f$  and calling this pressure head  $\psi$  yields the following.

$$\frac{\partial [\rho(S_m n_m + S_f n_f)]}{\partial t} + \nabla \cdot \rho(\bar{q}_m + \bar{q}_f) + \nabla \cdot \rho \bar{V}(S_m n_m + S_f n_f) = 0 \quad (5)$$

Thus, it is not necessary to evaluate  $\omega$ . Equation 5 may be expanded so that individual terms may be evaluated.

$$\begin{aligned} & \rho \frac{\partial \psi}{\partial t} \left\{ \left[ n_m \frac{\partial S_m}{\partial \psi} + n_f \frac{\partial S_f}{\partial \psi} \right] + \frac{1}{\rho} \frac{\partial \rho}{\partial \psi} (S_m n_m + S_f n_f) \right\} + \\ & \rho \left[ S_m \frac{\partial n_m}{\partial t} + S_f \frac{\partial n_f}{\partial t} \right] + \nabla \cdot \rho(\bar{q}_m + \bar{q}_f) + \\ & \rho(S_m n_m + S_f n_f) \nabla \cdot \bar{V} + \bar{V} \cdot \nabla [\rho(S_m n_m + S_f n_f)] = 0 \end{aligned} \quad (6)$$

The discussion of the evaluation of the terms in Eq. 6 will proceed from left to the right. The first two terms (terms containing " $n \partial S / \partial \psi$ ") represent the storage of water in the unit volume resulting from a change in saturation of the matrix and the fracture system. The matrix saturation and its partial derivative with respect to pressure can be experimentally determined in a variety of different manners including porosimetry tests using injection of mercury into the matrix and, more directly, using thermocouple

psychrometer tests. A comparison of these two methods and the results of extensive tests of matrix material may be found in the report by Peters et al. (1984). An example (taken from Peters et al. (1984)) of typical data resulting from psychrometer testing of matrix samples from unit TSW2 may be seen in Figure 5. The data from these tests may be fitted by a variety of functions, including those proposed by Haverkamp et al. (1977) and van Genuchten (1978). Peters found that either of the two functions yielded adequate fits if the data were well behaved and complete. However, the function developed by van Genuchten is analytically integrable in the equations used to calculate the unsaturated conductivity. Thus, it was chosen to fit all of the data in the report by Peters, and it also will be used in the rest of this paper.

$$S = (S_s - S_r) \left[ \frac{1}{1 + |\alpha\psi|^\beta} \right]^\lambda + S_r \quad (7)$$

The subscripts "s" and "r" refer respectively to the state of saturation at the saturated state ( $\sim 1$ ) and at the residual saturation. The parameters  $\alpha$  and  $\beta$  are the fitting coefficients that respectively influence the break point and the slope of the part of the curve where the saturation is changing rapidly.  $\lambda$  is defined as  $1 - 1/\beta$ . The equation is valid for pressure head ( $\psi$ ) values less than zero. The material is completely saturated for all pressure heads greater than zero.

Representative matrix saturation curves for units above the water table may be seen in Figure 6, which is reproduced from the report by Peters et al. (1984). This figure indicates that there are significant differences in the shape of the matrix saturation curve for the hydrologic units found above the water table at Yucca Mountain. Table 1 contains information concerning the fitting parameters used to construct these saturation curves as well as other information needed for hydrologic calculations.

Information regarding fracture saturation characteristics is much more scarce. Wang and Narasimhan (1985) have used statistical concepts to develop equations describing the saturation curve for fractures in a densely welded

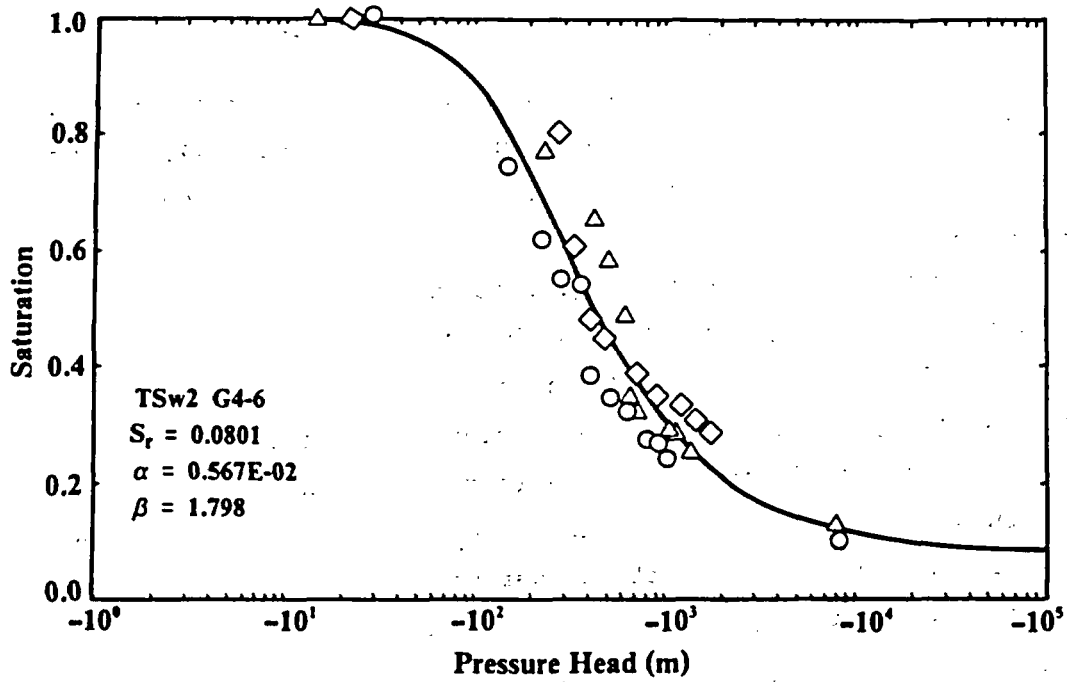


Figure 5. Saturation curve for sample G4-6 Taken from Unit TSw2.

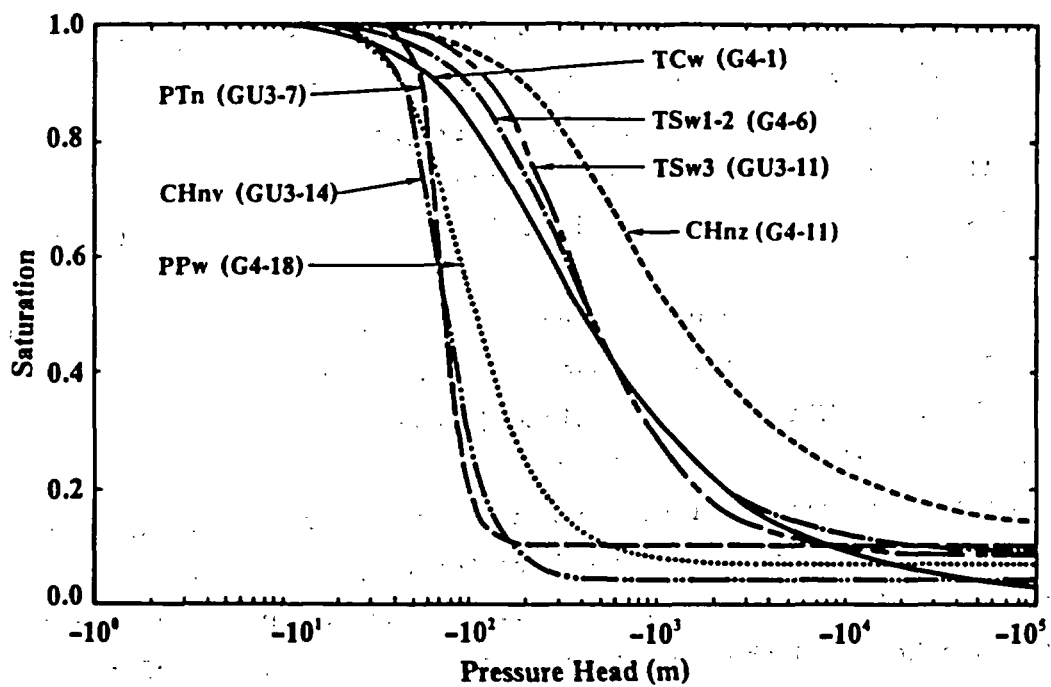


Figure 6. Representative matrix-saturation curves for the unsaturated-zone, hydrologic units.

tuff. Their fracture saturation curve is similar to that of a coarse sand such as that shown in Freeze and Cherry's text on page 42. Plans are being made to measure experimentally the saturation curves of fractured core (Klavetter et al., 1985).

The second set of terms in Eq. 6 (terms containing " $1/\rho \partial\rho/\partial\psi$ ") represents the storage of water in the unit volume due to the compressibility of water. The quantity  $1/\rho \partial\rho/\partial\psi$  is proportional to the water compressibility and is relatively constant. It will be denoted as  $\beta_w$ .

The third set of terms in Eq. 6 (terms containing " $S \partial n/\partial t$ ") represents the storage of water in the unit volume due to the net expansion of the matrix pores and the fracture apertures.

The fourth term represents the net change in flux of water that is withdrawn from the unit volume. The final two terms (terms containing " $\bar{V}$ ") represent the movement of water out of the unit volume due to movement of the rock mass (e.g., due to dilation).

The information and assumptions listed below as statements 1 to 6 were used in order to rewrite Eq. 6 in terms of one variable,  $\psi$ , the pressure head. The result is Eq. 8, which may be solved for the pressure head field, subject to the boundary conditions, material properties, etc.

- 1) The continuity equation for the matrix grain mass.
- 2) The three-dimensional bulk rock consolidation equation with the assumption that the displacement is vertical (see Reeves and Duguid (1975) for further discussion).
- 3) The assumption that a unit change in the quantity "total saturation times pressure head" at a point causes a unit change in the local stress field (see McTigue, Wilson, and Nunziato (1984)).
- 4) Darcy's equation for fluid flow.
- 5) Identical pressure head in the fractures and the matrix (previously discussed and used, but listed here for completeness).
- 6) The conventional assumption that total head is defined as the sum of the pressure head and the elevation above some reference surface.

Table 1. Unsaturated zone, hydrologic unit properties

Matrix Properties <sup>a</sup>							
Unit	Sample Code	Grain Density (g/cm <sup>3</sup> )	Porosity (n <sub>m</sub> )	Hydraulic Conductivity (K <sub>m,b</sub> ) (m/s)	S <sub>r</sub>	α (10 <sup>-2</sup> /m)	β
TCw	G4-1	2.49	0.08	9.7 x 10 <sup>-12</sup>	0.002	0.821	1.558
PTn	GU3-7	2.35	0.40	3.9 x 10 <sup>-07</sup>	0.100	1.50	6.872
TSw1	G4-6	2.58	0.11	1.9 x 10 <sup>-11</sup>	0.080	0.567	1.798
TSw2	G4-6	2.58	0.11	1.9 x 10 <sup>-11</sup>	0.080	0.567	1.798
TSw3	GU3-11	2.38	0.07	1.5 x 10 <sup>-12</sup>	0.080	0.441	2.058
CHnv	GU3-14	2.37	0.46	2.7 x 10 <sup>-07</sup>	0.041	1.60	3.872
CHnz	G4-11	2.23	0.28	2.0 x 10 <sup>-11</sup>	0.110	0.308	1.602
PPw	G4-18	2.59	0.24	4.5 x 10 <sup>-09</sup>	0.066	1.41	2.639

Fracture Properties <sup>c</sup>								
Unit	Sample Code	Horizontal Stress <sup>d</sup> (bars)	Fracture Aperture (microns)	Fracture Conductivity (10 <sup>-5</sup> m/s)	Fracture Density <sup>e</sup> (No./m <sup>3</sup> )	Fracture Porosity <sup>f</sup> (n <sub>p</sub> ) (10 <sup>-5</sup> )	Fracture Compressibility {∂n <sub>p</sub> /∂σ'} (10 <sup>-8</sup> /m)	Bulk Frac. Conductivity <sup>g</sup> {K <sub>f,b</sub> } (10 <sup>-9</sup> m/s)
TCw	G4-2F	1.1	8.74	3.8	20	14.	132.	5.3
PTn	G4-3F	3.3	27.0	61.	1	2.7	19.	16.
TSw1	G4-2F	9.5	5.13	2.2	8	4.1	5.6	0.80
TSw2	G4-2F	21.9	4.55	1.7	40	18.	12.	3.1
TSw3	G4-2F	29.9	4.34	1.6	10	4.3	2.1	0.69
CHnv	G4-4F	34.3	15.5	20.	3	4.6	2.8	9.2
CHnz	G4-4F	34.3	15.5	20.	3	4.6	2.8	9.2
PPw	G4-2F	39.2	4.16	1.4	3	1.3	.5	0.64

Fracture saturation coefficients are S<sub>r</sub>=0.0395, α = 1.2651/m, and β = 4.23

Unit	TCw	PTn	TSw1	TSw2	TSw3	CHnv	CHnz	PPw
Coefficient of consolidation <sup>h</sup> {α' <sub>bulk</sub> } (10 <sup>-7</sup> /m)	6.2	82.	12.	5.8	5.8	39.	26.	17.

The compressibility of water {β<sub>w</sub>} is 9.8 x 10<sup>-7</sup>/m

- Notes: a) All matrix data in this section are from Peters et al. (1984).  
 b) The matrix saturated conductivity and the bulk matrix saturated conductivity (K<sub>m,b</sub>) are essentially the same because the factor that converts the matrix value to the bulk matrix value (1-n<sub>p</sub>) is nearly equal to 1.0.  
 c) Unless noted otherwise, this fracture information is from Peters et al. (1984).  
 d) Horizontal stress assumed to be one-third the overburden weight, evaluated at average unit depth in USW G-4.  
 e) Based on the report by Scott et al. (1983).  
 f) Calculated as fracture volume (aperture times 1 square meter) times number of fractures per cubic meter.  
 g) This value of "K<sub>f,b</sub>" was obtained by multiplying the fracture conductivity by the fracture porosity.  
 h) Based on the report by Nimick et al. (1984).

$$\begin{aligned}
& \rho \frac{\partial \psi}{\partial t} \left\{ \left( n_m \frac{\partial S_m}{\partial \psi} + n_f \frac{\partial S_f}{\partial \psi} \right) + S'_w (S_m n_m + S_f n_f) + \right. \\
& \alpha'_{\text{bulk}} \frac{(S_m n_m + S_f n_f)}{n_m + n_f} (S_m - n_f (S_m - S_f)) \left. - \right. \quad (8) \\
& \left. \frac{\partial n_f}{\partial \sigma'} \frac{(S_m n_m + S_f n_f)}{n_m + n_f} (S_m - S_f) \right\} = \nabla \cdot \left[ \rho (\bar{K}_{m,b} + \bar{K}_{f,b}) \cdot \nabla (\psi + z) \right]
\end{aligned}$$

The quantity  $\alpha'_{\text{bulk}}$  is defined in bulk rock properties as:

$$\alpha'_{\text{bulk}} = \frac{(1 + \nu)(1 - 2\nu)}{E(1 - \nu)} \quad (9)$$

where E is the modulus of deformation and  $\nu$  is Poisson's ratio. The term  $\partial n_f / \partial \sigma'$  (giving the change in fracture porosity with stress) can be determined by experimentally measuring the closure of a fracture with increased stress (e.g., Peters et al., 1984).

The subscripts "m,b" and "f,b" on the conductivity variable "K" indicate that the matrix and fracture conductivities are bulk values for a unit volume of the fractured, porous media. These values may be estimated as the conductivity for the material times its relative volume in bulk material.

The functional dependence of the hydraulic conductivity on pressure head is very difficult to measure, especially when the matrix saturated conductivity may be less than  $10^{-11}$  m/s. There are some methods being explored which may show promise (e.g., matrix testing methods described by Johnson et al., 1959; and for fractures Klavetter et al., 1985); however, work in this area for tuffs with low permeabilities is currently in the preliminary stage. For the present, the hydraulic conductivity will be calculated. A variety of methods are available (e.g., Brooks and Corey, 1966; Burdine, 1953;

Mualem, 1976), and at present there is no indication whether any of these is superior to the others for predicting the unsaturated hydraulic conductivity for a hard rock such as tuff or even whether any of these do an adequate job of prediction. The method currently being used is that of Mualem because it gives results that are in the middle of those predicted by a variety of other methods (Klavetter and Peters, 1985), and it has been shown to yield better estimates of the unsaturated conductivity of a variety of unconsolidated materials than the other methods (Mualem, 1976). The hydraulic conductivity as a function of pressure head using the method of Mualem yields the following analytical expression when the saturation-curve fit of van Genuchten (Eq. 7) is used:

$$K(\psi) = K_s \left[ 1 + |\alpha\psi|^\beta \right]^{-\lambda/2} \left\{ 1 - \left[ \frac{|\alpha\psi|^\beta}{1 + |\alpha\psi|^\beta} \right]^\lambda \right\}^2 \quad (10)$$

$K_s$  is the saturated conductivity, a parameter that can be measured fairly easily.

For convenience in discussion and labeling of figures, the mathematical terms in the left side of Eq. 8 are named as follows.

$$\text{Matrix Sat.:} \quad n_m \frac{\partial S_m}{\partial \psi} \quad (8a)$$

$$\text{Fracture Sat.:} \quad n_f \frac{\partial S_f}{\partial \psi} \quad (8b)$$

$$\text{Water Comp.:} \quad \beta_w' (S_m n_m + S_f n_f) \quad (8c)$$

$$\text{Bulk Rock Comp.:} \quad \alpha_{\text{bulk}}' \left[ \frac{(S_m n_m + S_f n_f)}{n_m + n_f} (S_m - n_f (S_m - S_f)) \right] \approx \alpha_{\text{bulk}}' S_m^2 \quad (8d)$$

$$\text{Fracture Comp.:} \quad \frac{\partial n_f}{\partial \sigma'} \left[ \frac{(S_m n_m + S_f n_f)}{n_m + n_f} (S_m - S_f) \right] \approx \frac{\partial n_f}{\partial \sigma'} S_m (S_m - S_f) \quad (8e)$$

The coefficients on the left side of Eq. 8 (referred to as "capacitance coefficients") relate to the storage of water as  $\psi$  is varied. The first two terms on the left side (named above as Matrix Sat. and Fracture Sat.) correspond to the storage of water in the unit volume due to saturation of the matrix and the fracture system. The second group (named above as Water Comp.) corresponds to the storage of water due to the compressibility of water contained in the fractured, porous medium. The final group on the left side (Bulk Rock Comp. and Fracture Comp.) represents the storage of water due to dilation of the bulk rock. The term on the right side is proportional to the divergence of the total water flux moving through the unit volume.

The capacitance coefficients found on the left side of Eq. 8 have a strong functional dependence on the pressure head  $\psi$ . Each group of terms from Eq. 8 is plotted in Figures 7-9 for one unit from each of the previously described rock types (Nonwelded, vitric tuffs - PTn; Densely welded tuffs - TSw2; and Nonwelded, zeolitized tuffs - CHnz). The labels used in the figures are defined above.

In the last two coefficients (Eq. 8d and 8e), the terms containing  $n_f$  may be neglected because, in most cases,  $n_f$  is of the order of  $10^{-5}$  (see Table 1 and Snow (1970)) and the term  $S_m - S_f$  is no greater than 1. The values of the parameters that were used to produce Figures 7-9 are listed in Table 1 and are thought to be representative of Yucca Mountain. One should note that the "Fracture Comp." term in Eq. 8 and plotted in Figures 7-9 is subtracted from the sum of the other four terms.

Inspection of these figures indicates some results that may not be entirely expected. The maximum value of the fracture-saturation coefficient for unit TSw2 is of the same order of magnitude as the maximum value of the matrix-saturation coefficient because the relatively small volume of the fractures is assumed to saturate over a very small change in pressure head. It is the largest parameter in the pressure region between -0.1 and -1.0 meters for all units. The matrix-saturation coefficient dominates over almost all of the rest of the pressure-head range except where the matrix is saturated or is at its residual saturation. For pressure heads where both the fractures and matrix are totally saturated or both are nearing their residual saturation ( $\psi$  greater than about -0.01 m and  $\psi$  less than about  $-10^4$  m)

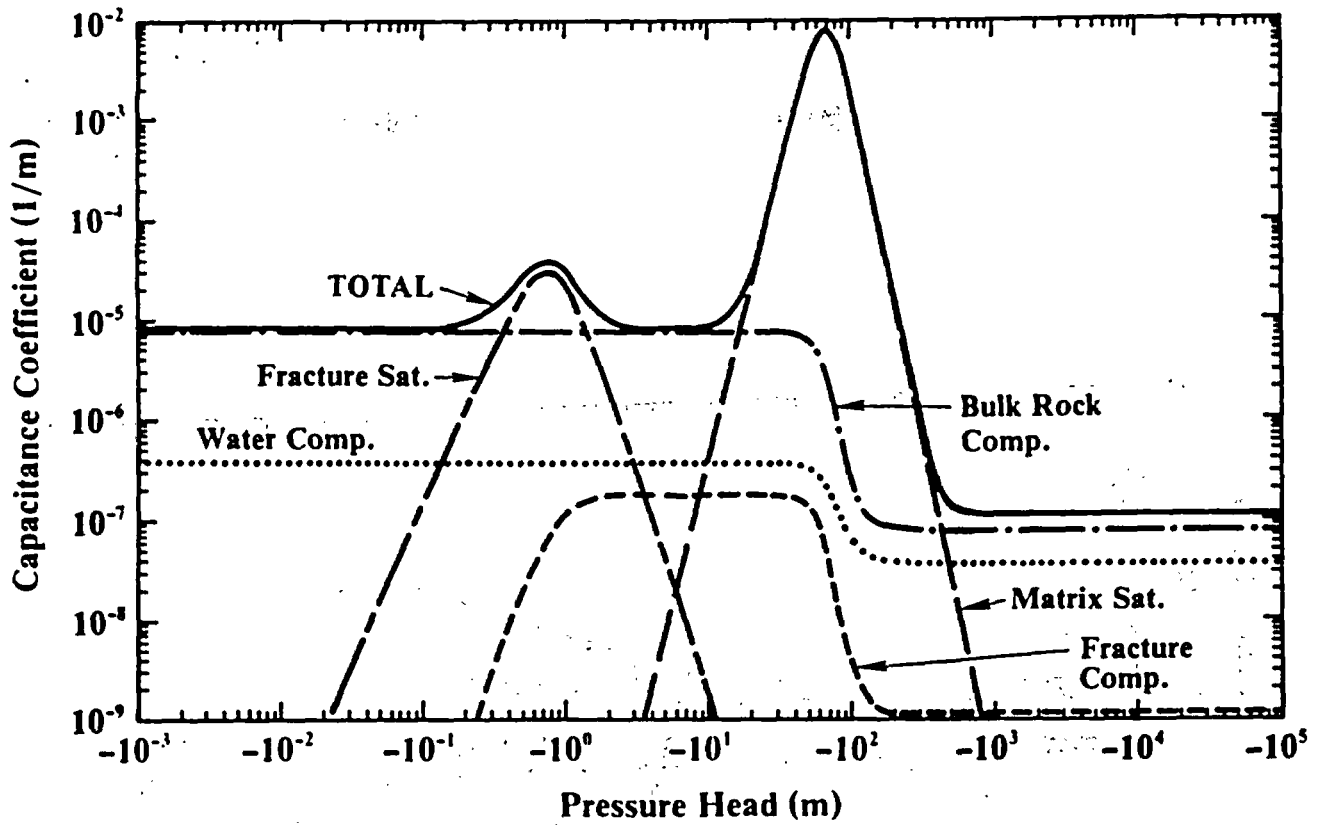


Figure 7. Capacitance coefficients for Unit PT'n.

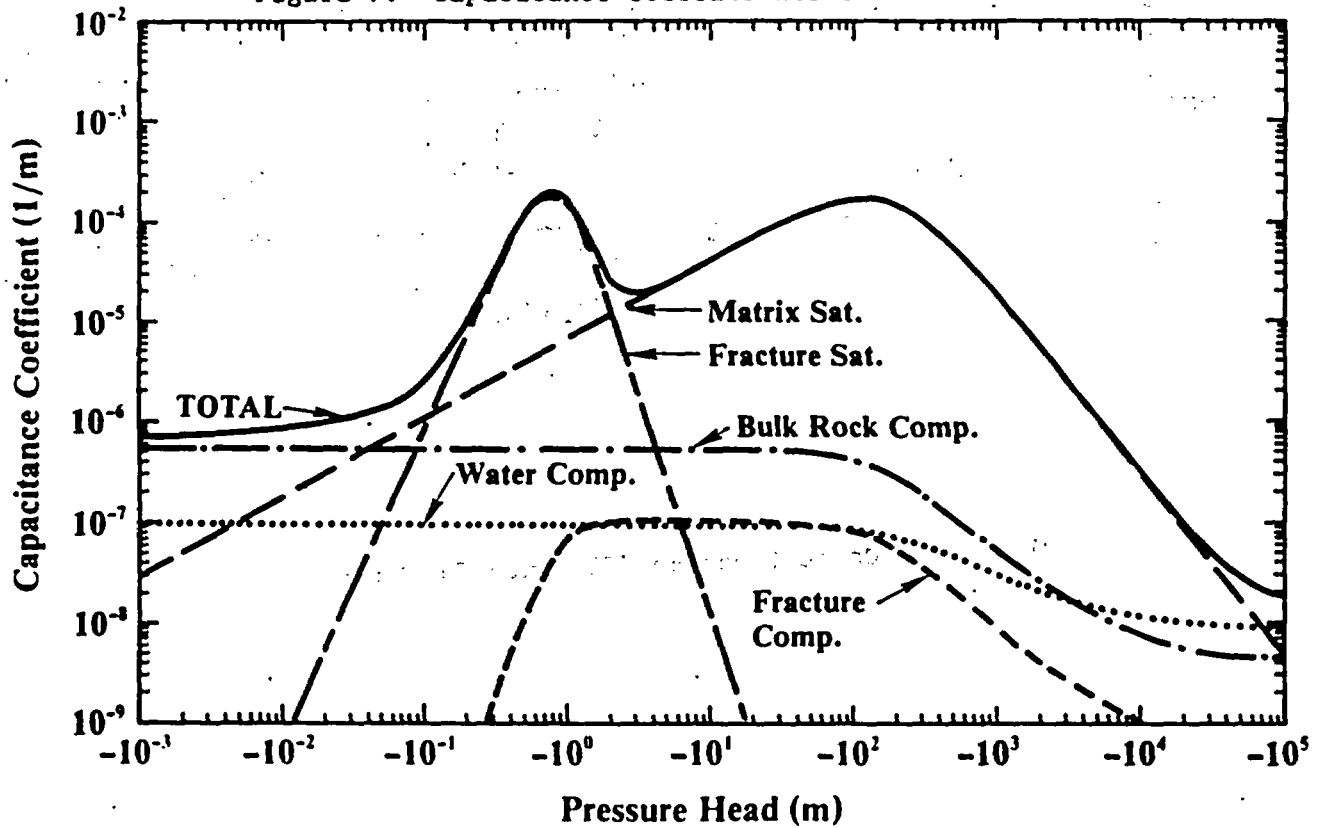


Figure 8. Capacitance coefficients for Unit TSw2.

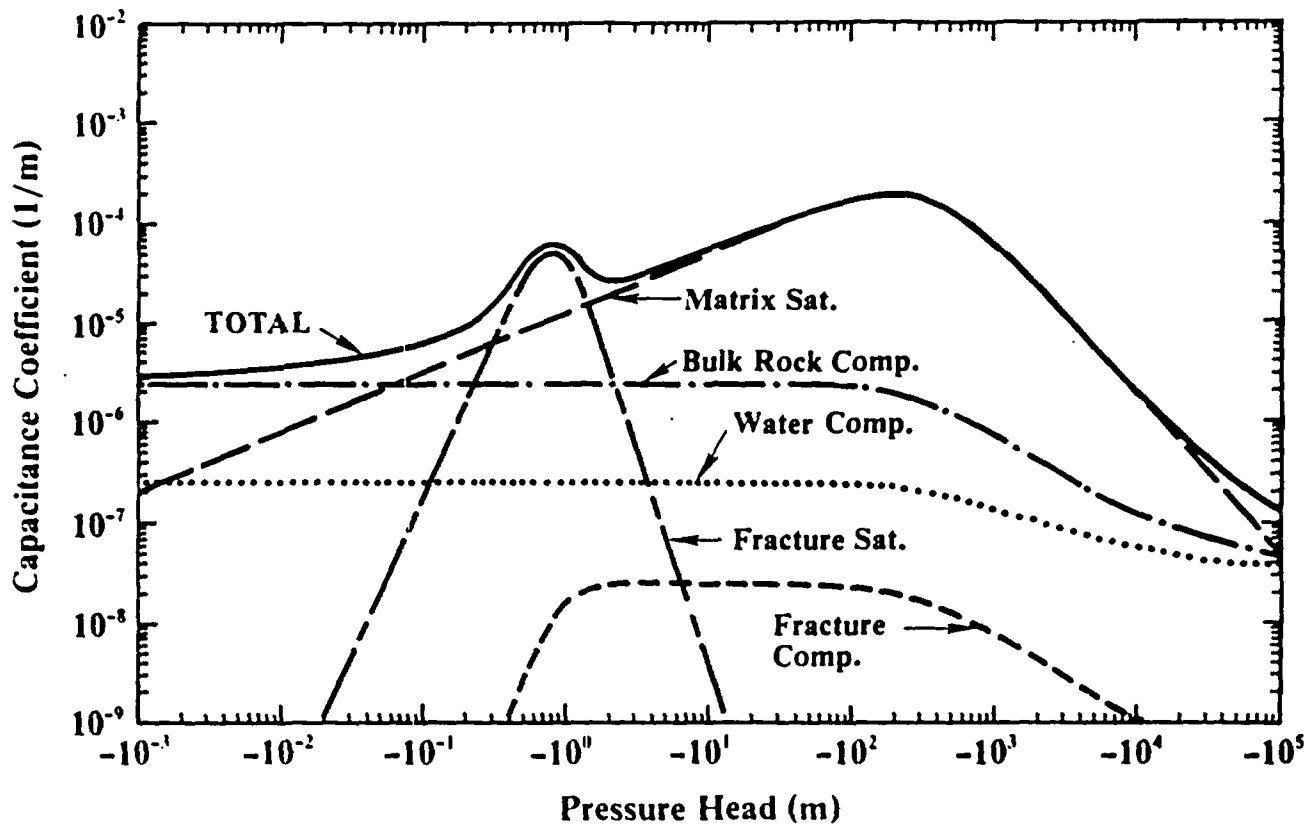


Figure 9. Capacitance coefficients for Unit CHnz.

the major coefficient may be the bulk rock compressibility (e.g., Fig. 7), which accounts for storage of water due to rock deformation. The value for the bulk-rock-compressibility coefficient near a pressure-head value of zero is probably reasonable. At large negative pressure heads its value and even the assumptions used in deriving its functional form at that extreme are in doubt. However, few hydrological problems of interest will be run at pressure heads where both the matrix and fractures are desaturated.

The terms on the right side of the Eq. 8 are also highly variable with the pressure head  $\psi$  because of changes in the saturation of the matrix and the fractures. Figures 10-12 show the conductivity curves for a unit volume containing only "fracture material," a unit volume of matrix material, and a unit volume containing both materials for one of each of the three rock types previously discussed. This last line represents the conductivity curve of the fractured, porous media ( $K_{m,b} + K_{f,b}$ ) where  $K_{f,b}$  is calculated as the fracture conductivity times the fracture porosity and  $K_{m,b}$  is calculated as the matrix conductivity times the quantity one minus the fracture porosity.

The total conductivity curves plotted in Figures 10-12 contain either one or two plateaus of fairly constant conductivity with rapidly changing conductivity in the remaining portions of the curve. Curves containing two plateaus result from units which have low matrix conductivity and relatively high fracture conductivity (e.g., units TSw2 and CHnz). Total conductivity curves for these units are nearly constant at pressure-head values where the fractures are saturated ( $\psi < -1$  m) and in the pressure-head range where the fractures are at their residual saturation but the matrix is still saturated (from about -1 m to of the order of -10 to -100 m). In the regions where the saturation is changing, the conductivity changes very rapidly. Curves containing a single plateau result from units that have relatively low fracture conductivities and high matrix conductivities (e.g., PTn). The total conductivity is essentially that of the matrix over the entire range of pressure head; thus, the curve has a much simpler shape. The values of the parameters that were used to produce Figures 10-12 are listed in Table 1 and are thought to be representative of Yucca Mountain.

Equation 8 may be solved numerically for the pressure head with values specified for the material properties (which were discussed above), boundary

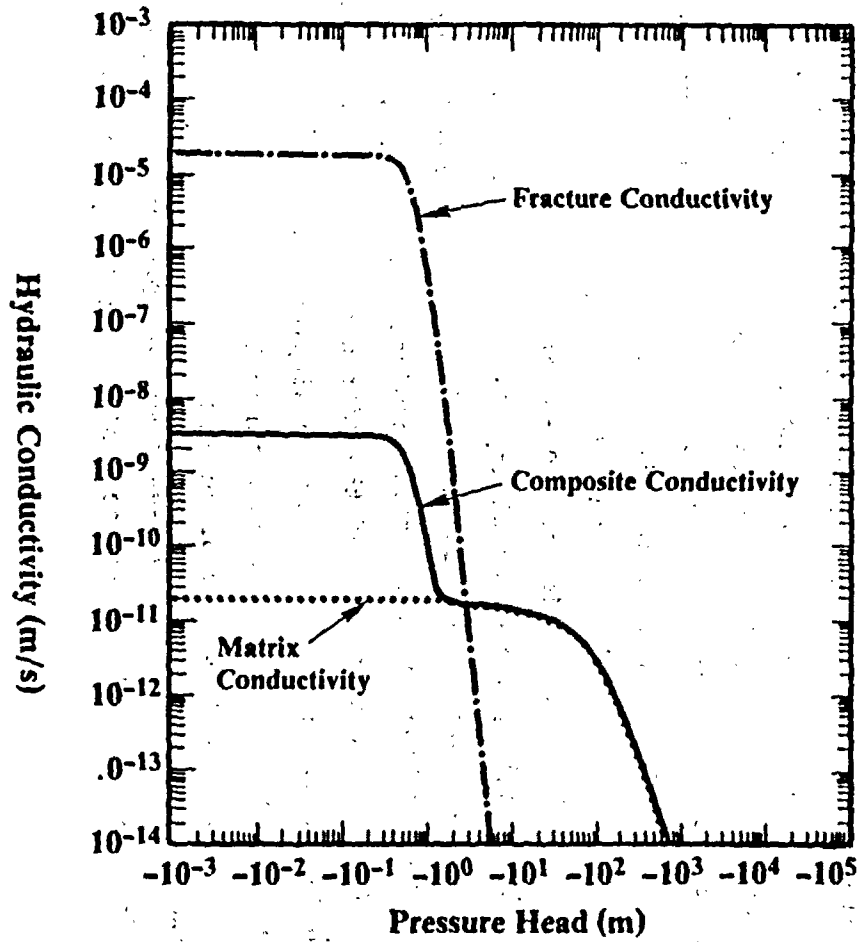


Figure 11. Conductivity curve for Unit TSw2.

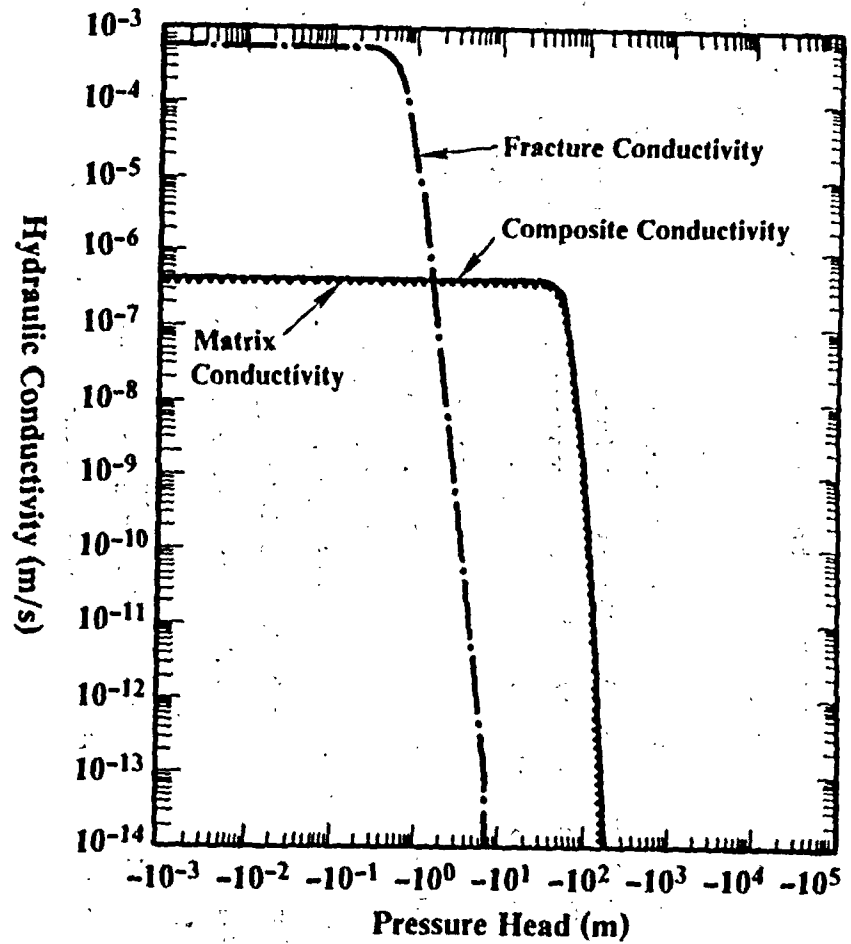


Figure 10. Conductivity curve for Unit PTn.

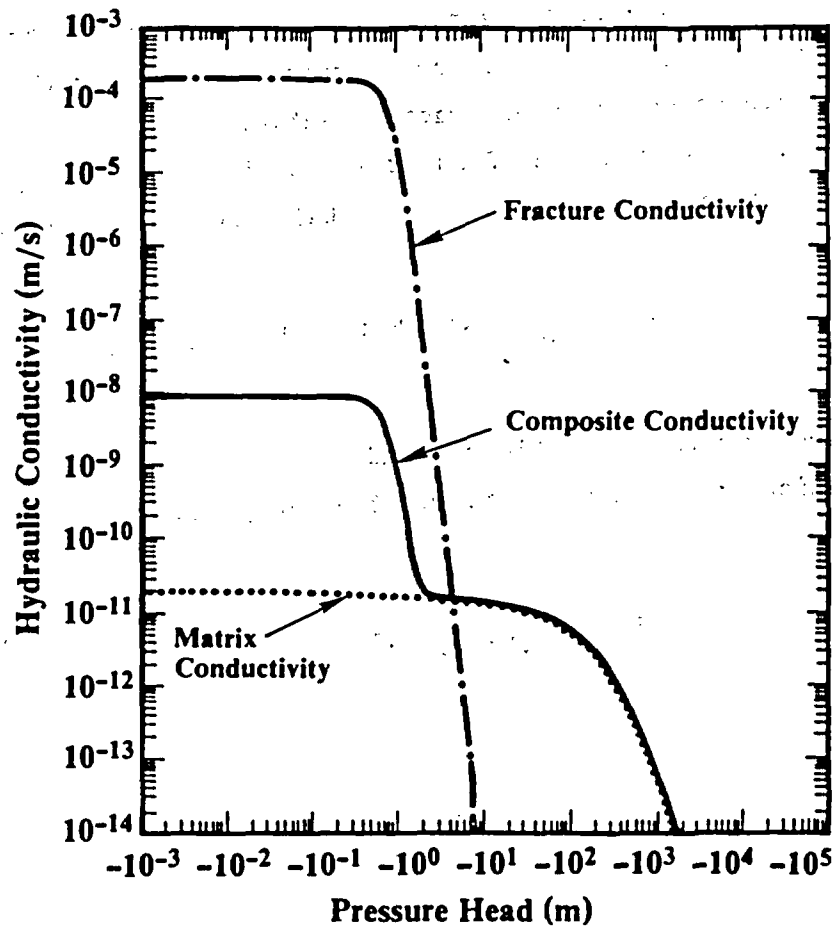


Figure 12. Conductivity curve for Unit CHnz.

conditions (e.g., fluxes and pressure heads), and an initial condition. The individual flux in the matrix and fractures may then be calculated using Darcy's law individually for the matrix and the fracture system. The velocity used in transport equations may be calculated by dividing the flux by the area through which each flows (e.g., the appropriate area for the fractures would be the fracture porosity times fracture saturation).

The steady-state version of Eq. 8 is obtained by setting the left side to zero. This then can be integrated to obtain the following form of Darcy's law:

$$- [\bar{K}_{m,b} + \bar{K}_{f,b}] \cdot \nabla(\psi + z) = \bar{q}_m + \bar{q}_f = \bar{q}_{total} \quad (11)$$

Note that some terms in Equations 8 and 11 may be summed, yielding Equations 12 and 13 which are written in terms of a "composite-porosity" material.

$$\rho \frac{\partial \psi}{\partial t} \left[ n_c \frac{\partial S_c}{\partial \psi} + \beta'_w n_c S_c + \alpha'_{bulk} S_c^2 \right] = \nabla \cdot [\rho \bar{K}_c \cdot \nabla (\psi + z)] \quad (12)$$

$$- \bar{K}_c \cdot \nabla(\psi + z) = \bar{q}_c \quad (13)$$

The subscript "c" refers to the composite-porosity material, which is equivalent to the fractured, porous matrix system in terms of predicting the total fluxes and the pressure-head field. This model (Equations 12 and 13) is informally referred to as a "composite-porosity" model. (The term containing the partial derivative of the fracture porosity with respect to the stress has been neglected because it has been shown previously in this paper to be small in comparison with the other terms.) The definition of the terms in Equations 12 and 13 follows:

$$n_c \frac{\partial S_c}{\partial \psi} \equiv n_m \frac{\partial S_m}{\partial \psi} + n_f \frac{\partial S_f}{\partial \psi} \quad (14)$$

$$n_c S_c \equiv n_m S_m + n_f S_f \quad (15)$$

$$S_c \equiv n_c S_c / (n_f + n_m) \approx S_m \quad (16)$$

$$\bar{k}_c \equiv \bar{k}_{m,b} + \bar{k}_{f,b} \quad (17)$$

The definition of the the composite-porosity model terms in Eq. 15, 16, and 17 corresponds exactly to the quantities that would be obtained from volume-averaging the properties of the fracture and matrix system; the definition of the other term differs slightly. The volume-averaged value of  $n_c (\partial S_c / \partial \psi)$  approaches the composite-porosity definition in Eq. 14 as the compressibility of the matrix and fractures becomes small in comparison with the derivative of the saturation of the matrix and fractures; this condition is approximately true at Yucca Mountain. (As previously discussed, we may neglect the term  $n_f (S_f - S_m)$ .)

The derivation presented above follows that of many other authors, as previously mentioned. Its main difference is the crucial assumption, based on information relevant to Yucca Mountain, that the pressure heads in the fractures and matrix are identical. If this assumption is made initially, then Eq. 8 can be derived in an alternative manner assuming that the matrix pore system can be extended to include the "fracture pores." This alternative derivation of Eq. 8 is the subject of the following section.

## Microscopic Derivation of the Flow Equation

The theoretical derivation in the previous section produced a macroscopically based model that assumes that the fracture and matrix hydrologic properties used are statistically "representative" of a large volume of rock mass. The hydrologic parameters for the fractures and matrix are combined to estimate rock mass properties for the composite material. In Eq. 12 above, that is the equation of motion for a fluid in a composite-porosity material, the major hydrological parameters which must be determined are 1) the saturation of the composite rock mass as a function of the pressure head,  $S_c(\psi)$  and 2) the relative conductivity tensor for the composite rock mass,  $\bar{K}_c(\psi)$ . Experimental results from a large number of samples, combined with the assumption of a constitutive equation that describes the water movement characteristics in either the matrix system or the fracture system, are used to determine a statistically representative set of hydrologic property values for each system. The hydrological parameters so determined for the fractures and matrix are combined as postulated in the above model to represent the coefficients in the single equation, Eq. 12, for fluid motion in a composite material.

However, a microscopic approach, using the actual physical structure of the system of interest combined with fundamental theory of fluid flow in pores of a specific geometry, can also be used to determine relative conductivity and saturation values as a function of pressure head for the rock mass. In this approach, the contributions of the individual matrix pores and fractures for a volume of rock mass are combined to determine the hydrologic parameters for the composite rock material. Here, the fractures are treated as large "pores." The hydrologic parameters can then be used in the desired constitutive equation to describe flow in a single continuum. The continuum consists of matrix and fractures, with the fractures assumed to be uniformly distributed throughout the rock-mass volume of interest. If the rock is assumed to be rigid, Richards' equation, Eq. 1 (Richards, 1931) may be used to calculate flow in an unsaturated medium. The equation would be written for the rock-mass continuum consisting of matrix and fractures with hydrologic parameters required for the composite medium. One could also choose to include compressibilities of the water and rock in the constitutive equation

for the composite medium. If terms that include fracture porosity are generally assumed to be insignificant as a lower-order effect, then Eq. 12 results. The difficulty in using Eq. 12 arises from the problems in estimating the hydrologic parameters for the composite medium. The previous section derived the constitutive equation for the rock mass and a method for estimating the rock-mass unsaturated, hydrologic properties from data on the individual matrix unsaturated properties and fracture unsaturated properties. The remainder of this document will focus on the development of another method by which the necessary hydrologic parameters in Eq. 12 can be estimated for a fractured rock mass. The relative conductivity and saturation versus pressure head curves calculated by the two methods will be compared.

The previous derivation explicitly assumed the equality of the fracture and matrix pressure head along a direction perpendicular to flow; the approach here inherently assumes that the pressure head in the "large fracture pores" and in the small matrix pores are equal along a direction perpendicular to flow. The values for saturation as a function of pressure head and relative hydraulic conductivity as a function of pressure head (or saturation), which are determined independently of the flow equation in which they are to be used, can then be applied in Eq. 12 to describe the movement of fluid in a fractured, porous medium. Thus, two different methods are available to evaluate the terms  $S_c(\psi)$  and  $\bar{K}_c(\psi)$  in the flow equation for a fractured rock mass.

According to basic capillary theory, the pore sizes of the matrix determine their contribution to the saturation and the relationships between the relative hydraulic conductivity and pressure head. The distribution of fracture aperture sizes determines the contribution of the fractures. The curves calculated here are based upon available fracture and matrix data and are compared with the composite saturation-versus-pressure head and relative-hydraulic-conductivity curves calculated by the macroscopic formulation derived in the previous section. The fracture (and matrix) porosities were kept the same for both approaches. Composite curves postulated by the two formulations were compared quantitatively and qualitatively for the following three stratigraphic units (the depth in

parentheses corresponds to the sample depth in drill hole USW G-4 on the NTS from which the matrix hydrologic properties were determined). All of the units in the list below are above the water table at Yucca Mountain.

- 1) Topopah Spring Welded Unit [Non-Lithophysal Zone] (1158 ft)
- 2) Basal Vitrophyre of the Topopah Spring Welded Unit (1299 ft)
- 3) Calico Hills Nonwelded Unit (1548 ft)

The pore-size distribution data for samples of tuff matrix were obtained from mercury intrusion tests. A distribution of pore radii was obtained, along with the percent volume of the sample associated with each pore radius. A frequency plot of incremental volume versus pore diameter for a matrix sample obtained from drill hole USW G-4, 1158 ft, is shown in Figure 13 as an example. For most tuff samples for which mercury-intrusion data were available, there was little or no pore volume for pore radii above 1-5 micrometers, with the average, volume-based pore diameter for tuffs determined to be generally less than 0.1 micrometer.

Because no field information is available on the general distribution of fracture apertures in the various stratigraphic units in Yucca Mountain, a lognormal distribution was assumed. Snow (1970) notes that many arguments indicate the suitability of a lognormal distribution for describing fracture-aperture frequencies in rock. He has studied joints in granite outcrop and found that mean apertures were distributed approximately lognormally and suggests that apertures are similarly distributed at depth. Sharp (1970) measured apertures in a single fracture in the laboratory. The data showed a lognormal form, with a truncated tail due to the small area available for sampling. The two-parameter lognormal distribution (Aitchison, 1957) is defined by

$$f(b) = \left[ b(2\pi\sigma^2)^{1/2} \right]^{-1} \exp \left[ -(2\sigma^2)^{-1} (\ln b - \xi)^2 \right] \quad (18)$$

where  $f(b)$  is the frequency at between aperture  $b$  and  $b + db$ ,  $\xi$  is the mean aperture, and  $\sigma$  is the variance.

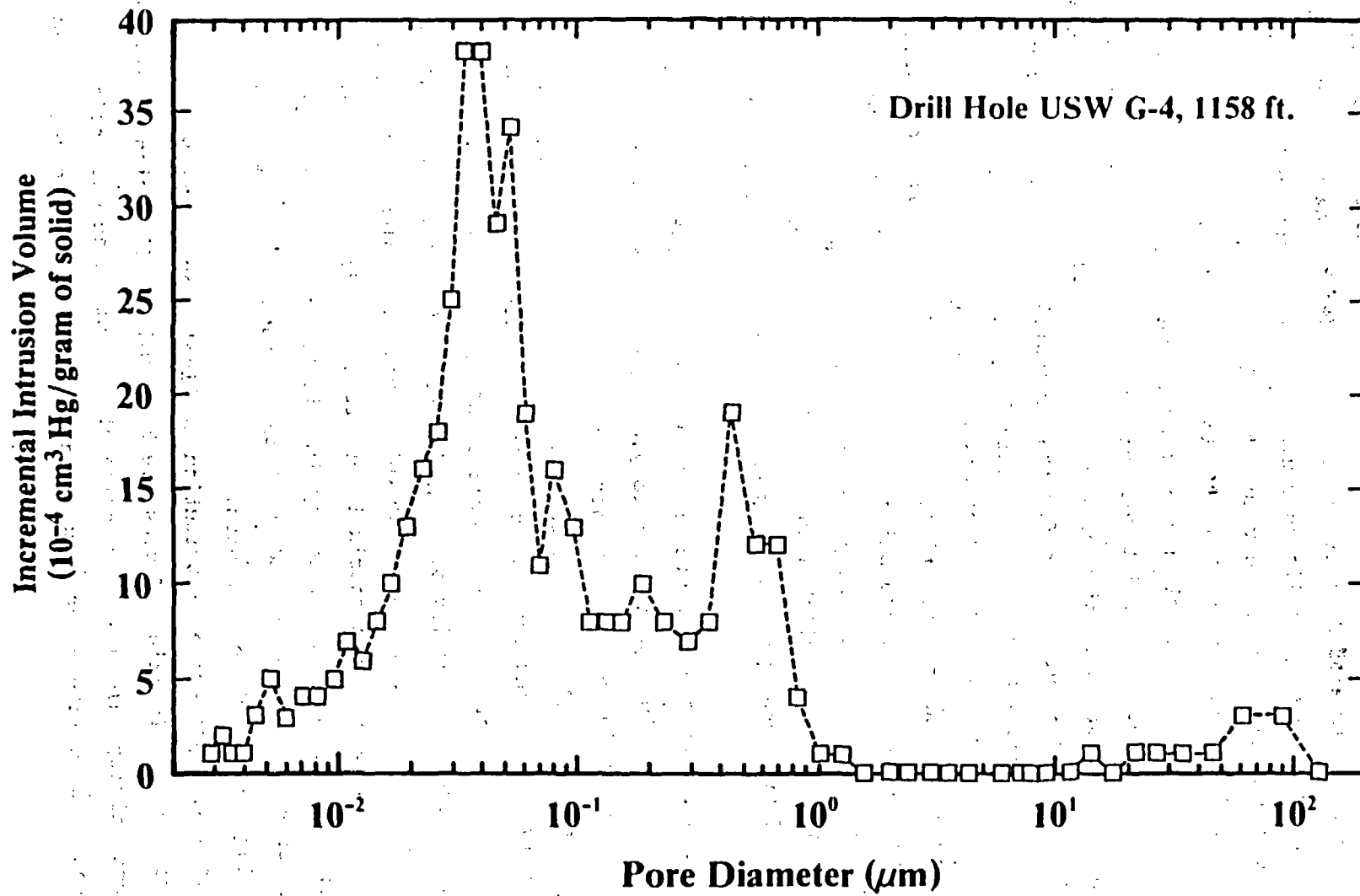


Figure 13. Incremental volume versus pore diameter for sample G4-6 from Unit TSw2.

For the stratigraphic units cases modeled with the microscopic approach, a fracture aperture value of 25 micrometers was chosen as the mean aperture. The average, equivalent hydraulic apertures in Table 1 are in the range of 4-27 micrometers. However, these values take into account the tortuosity of the fractures, both microscopic (surface topology) and macroscopic. Barton et al. (1983) noted that in this range of apertures, the physical aperture dimension is on the order of 2-7 times the equivalent, hydraulic aperture. Because the effects of tortuosity of the pores are included in the calculation of the relative conductivity curve for the composite pore-size distribution, the tortuosity effect inherent in the equivalent, hydraulic aperture was removed. Thus, an average value of 25 micrometers was used for the mean physical aperture as an approximation. A variance of 0.3 was arbitrarily chosen, because it seemed to approximate the variance of the fracture relative permeability curve assumed in the previous macroscopic approach. No information is currently available to determine the variance of the distribution of fracture apertures in the various stratigraphic units at Yucca Mountain.

The information on the aperture and pore-size distributions was combined with estimates of fracture porosities to yield a rock mass, "pore"-size distribution that includes both the matrix and fracture structural characteristics. The individual distributions were linearly weighted with their respective matrix and fracture porosities to create the cumulative, normalized volume distribution as a function of pore diameter (or radii). For example, for a fracture porosity of 10%, the pores with apertures in the range of 1-100 micrometers compose 10% of the total rock mass volume. The term "pore" refers here to either a matrix interstitial opening or a fracture opening. As explained below, tortuosity distributions for the resulting pore-size distributions were assumed, with the tortuosity of a pore decreasing with increasing pore aperture or radius.

With a composite pore-size distribution available for the rock mass, saturation values as a function of pressure head and one-dimensional relative hydraulic conductivity values as a function of pressure head were calculated. The adjustment to calculate water saturation as a function of pressure head

and pore radii can be based upon capillary bundle theory (e.g., see Hillel, 1982). From capillary theory, the pressure head,  $\psi$ , can be related as follows to the individual pore radius,  $r$ , for a fluid:

$$\psi = \frac{2\gamma \cos \phi}{\rho g r} \quad (19)$$

where  $\gamma$  is the surface tension between the solid and fluid,  $g$  is the acceleration due to gravity, and  $\phi$  is the fluid contact angle between the solid and fluid. If the pore-size distribution was conventionally determined from mercury-intrusion data, the mercury-intrusion pressure,  $P_{Hg}$ , for a particular pore size (and thus saturation) can be converted into equivalent water pressure-head by combining the relationships for both water and mercury to give

$$\psi_w = \frac{-P_{Hg}}{\rho_w g} \frac{\gamma_w \cos \phi_w}{\gamma_{Hg} \cos \phi_{Hg}} \quad (20)$$

The subscripts "w" and "Hg" refer to water and mercury, respectively. The specific values used for surface tension and contact angle were estimates based upon information contained in a variety of sources (e.g., Hillel, 1982) and are listed below.

$$\begin{aligned} \gamma_w &= 0.072 \text{ N/m} & \phi_w &= 15 \text{ degrees} \\ \gamma_{Hg} &= 0.484 \text{ N/m} & \phi_{Hg} &= 130 \text{ degrees} \end{aligned}$$

The water saturation corresponding to the adjusted water pressure head is 1 minus the mercury saturation at a particular pore radius determined from the intrusion tests. Thus, at zero pressure, no mercury has intruded into the pore volume, the mercury saturation is zero, and the corresponding water saturation is one. At the maximum recorded mercury pressure, corresponding to about  $-10^4$  m of water, the mercury content in the pore volume is a maximum, and the mercury saturation is assumed to be 100%, with a corresponding water saturation of zero.

Although fracture apertures are large in comparison with the pore radii sizes, the fracture system has an extremely low porosity (volume) in comparison to the matrix porosity. Thus, the fracture system has negligible effect on the saturation-versus-pressure-head curve calculated for the matrix-fracture system. The relative hydraulic conductivity curve is much more sensitive to the effects of fractures and is therefore more applicable to the comparison here of the "microscopic" model for a composite rock material to the "macroscopic" model presented in the previous section.

The relative hydraulic conductivity curve for the wetting phase can be calculated using the method of Burdine (1953). Burdine used capillary theory, along with assumptions on the effects of tortuosity of the pores on fluid flow, to formulate an equation to calculate wetting-phase relative hydraulic conductivity as a function of saturation or pore size. Burdine's contribution was primarily in his treatment of the tortuosity. A simplified formulation of Burdine's equation follows:

$$K_{rel} = \frac{n_{total}}{8k_s} \sum_{i=0}^{r_{max}} \frac{(S_w - S_{w,r})^2}{(1 - S_{w,r})^2} \frac{v(r_i)r_i^2}{\chi^2(r_i)} \quad (21)$$

where  $K_{rel}$  is the wetting-phase, relative permeability or relative hydraulic conductivity (dimensionless),  $k_s$  is the permeability ( $m^2$ ),  $r_i$  is the pore entry radius (m),  $v$  is the incremental volume fraction (dimensionless),  $n_{total}$  is the porosity,  $S_w$  is the saturation of the wetting phase,  $S_{w,r}$  is the irreducible saturation (residual saturation) of the wetting phase, and  $\chi(r_i)$  is the tortuosity factor of the sample. The pressure head associated with a particular saturation can again be determined from capillary theory by relating a pore size with its pore entry pressure, as noted by Eq. 19.

Rose (1949) and Wheeler (1955), among others, have suggested that the tortuosity factor for a sample is actually represented by a distribution of tortuosity factors, dependent upon the radius of the pore. Rose and Wheeler postulated an exponential form for this distribution, where the tortuosity decreases with increasing pore size. The exponential function suggested by

Rose for a sandstone was used here in the absence of any other information. Tortuosity distributions for tuff samples, as for any other real material, must be determined experimentally. The exponential distribution function used by Rose for sandstone is given by (with the pore radius in micrometers)

$$\chi(r_i) = A \exp(-Br_i) + C \quad (22)$$

The parameter 'B' appears to be related to how rapidly the cumulative pore volume changes with pore radius. 'C' is related to the tortuosity of the larger pores (fractures), or more properly the surface roughness characteristics that give rise to the differences between the physical fracture aperture and the effective, hydraulic aperture. The sum of 'A' plus 'C' is related to the maximum tortuosity of the smallest pore size. Equation 20 is the functional form for the tortuosity distribution used in Eq. 21.

For the three stratigraphic units mentioned previously, the composite relative conductivity curves, as calculated in the previous section with the "composite-porosity" model, are compared with the composite relative conductivity curves calculated from the pore size distribution data of the matrix and the assumed lognormal aperture distribution for the fractures. The comparisons are shown in Figures 14-16 with the fracture porosities noted. Constant values of 25 micrometers and 0.3 were used in the lognormal aperture distribution for the mean aperture and variance, respectively. The curves are not only qualitatively the same, but match quantitatively at most points. The pressure head at which the fracture conductivity becomes significant matches well between the two formulation methods. The saturation and relative conductivity relationships as a function of pressure head for the unsaturated rock mass can be substituted in Eq. 12 to describe flow in the fractured, porous media. This yields the same equation for flow as that derived in the previous approach with essentially equivalent values determined by both approaches for the required hydrologic properties.

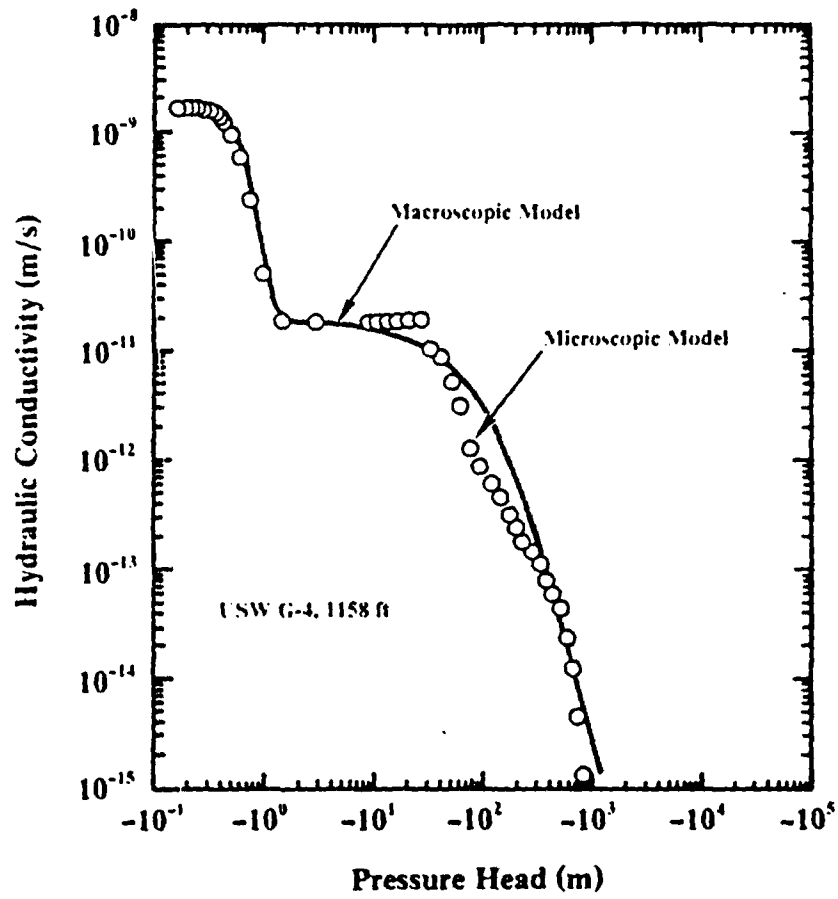


Figure 14. Hydraulic conductivity comparison for material representative of Unit TSw2.

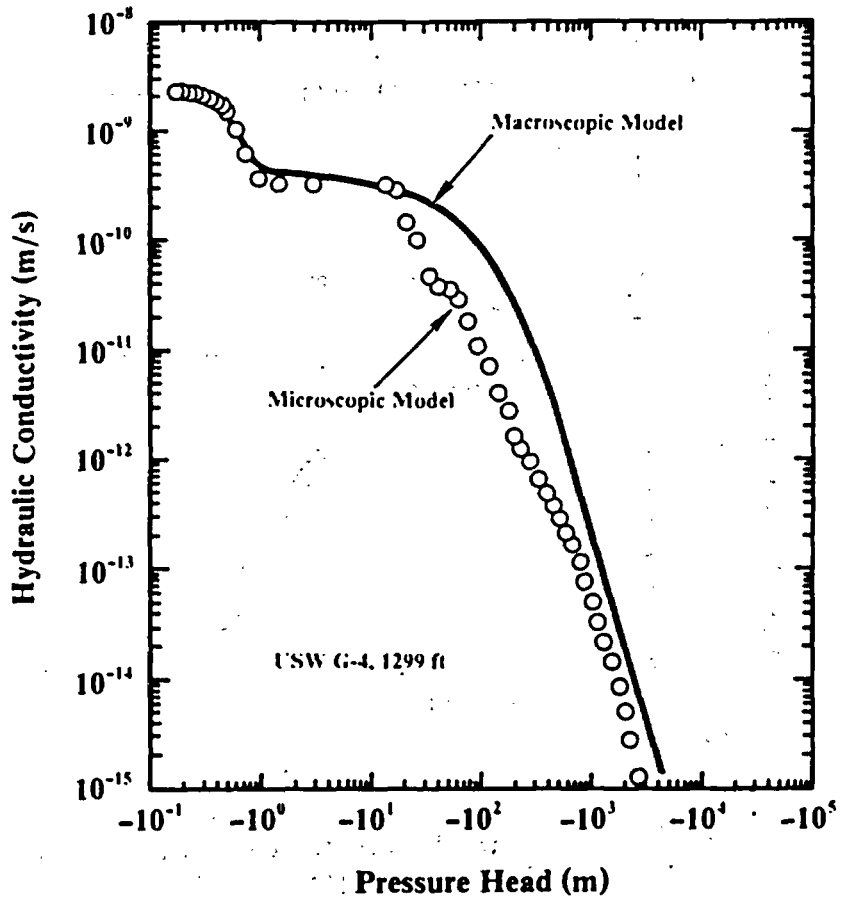


Figure 15. Hydraulic conductivity comparison for material representative of Unit TSW3.

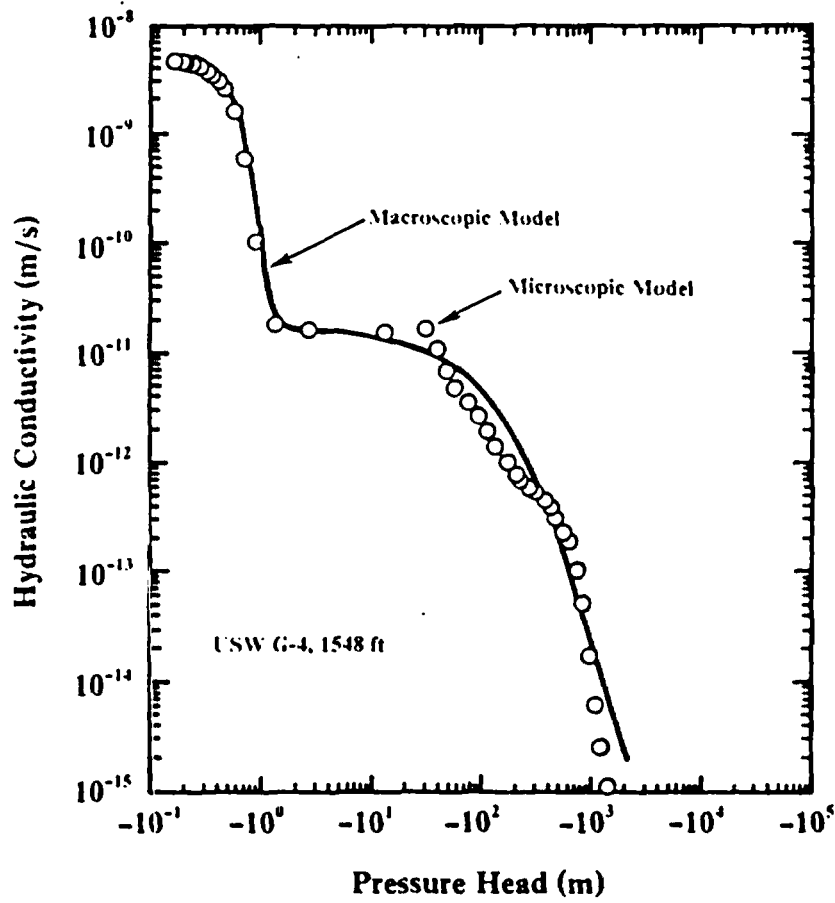


Figure 16. Hydraulic conductivity comparison for material representative of Unit CHnz.

Better quantitative agreement between the results of the two formulations was obtained by adjusting the values of 'A' and 'C' in Eq. 22 for the different samples. A constant value of 0.4 was suggested by Rose (1949) for sandstone for the parameter 'B' and was used in the absence of other information. The values of 'A' and 'C' used for the three comparisons are shown in Table 2. The small values of 'C' are indicative of the fact that overall fracture geometry resembles two parallel plates. Tortuosity factors for porous matrix materials such as sandstones and reaction catalysts are generally in the range of ~1-10, (Froment and Bischoff, 1979) although the magnitude of the pore sizes and the mean pore radii of tuffs are much smaller than those of sandstones or catalysts, and larger tortuosity factors might be expected. However, no definitive interpretations about the tortuosity distributions for tuff should be made from such a small sampling of results because of the complexities involved with the concept of tortuosity. Lumped into the tortuosity distribution are such parameters as pore-length distributions, pore shape, and connectivity between pores of different radii. The tortuosity distribution parameters should be experimentally determined for each porous medium of interest. No information is available for tuffs; therefore, parameters were used that provided a reasonable quantitative fit. The purpose of this comparison was not to determine tortuosity parameters but to qualitatively compare the two formulation methods for determining a rock mass relative hydraulic conductivity curve. The selection of tortuosity parameters does not affect the qualitative comparison of the curves.

---

Table 2 Coefficients for Tortuosity Exponential Distribution Function (Equation 22)

<u>Sample Code</u>	<u>Unit</u>	<u>A</u>	<u>B</u>	<u>C</u>
G4-6	TSw2	10.5	0.4	3.5
G4-8	TSw3	1.2	0.4	3.2
G4-11	CHnz	9.0	0.4	1.6

---

The excellent qualitative and quantitative comparison of the two methods for calculation of a relative conductivity curve for a rock mass adds confidence to the validity of the "composite-porosity" model assumptions presented earlier. The method presented here for the calculation of the curves is based upon available physical data on the structural characteristics and properties of the matrix and fractures and compares favorably with the macroscopic formulation presented. As more laboratory and field data become available on the distribution of fracture apertures and fracture porosities in the stratigraphic units of Yucca Mountain, these composite relative conductivity curves can be adjusted to provide a more realistic representation of the hydrologic system there.

#### SUMMARY

The prospective repository location at the Yucca Mountain site is in the unsaturated zone. The unsaturated zone contains high- and low-conductivity nonwelded tuffs, and low-conductivity, highly fractured tuffs. Hydrologic calculations using models that explicitly treat the fractures are not feasible because of the large number of fractures ( $\sim 10^{10}$ ) contained in a site-scale problem and the complexity of the fracture geometry. A continuum approach to calculating water flow in a fractured, porous medium was developed. The major assumption in this development was that the pressure heads in the fractures and the matrix are identical in a direction perpendicular to flow. Calculations of small-scale problems that explicitly zone in the fractures show that this assumption is correct at Yucca Mountain. Evaluation of the coefficients in the fluid continuity equation using both macroscopic and microscopic approaches yields qualitatively and quantitatively similar results.

## REFERENCES

- Aitchison, J., and J. A. C. Brown. 1957. "The Lognormal Distribution," Cambridge, University Press.
- Barenblatt, G. I., Iu. P. Zheltov, and I. N. Kochina. 1960. "Basic Concepts in the Theory of Seepage of Homogeneous Liquids in Fissured Rocks [Strata]," PMM, Vol. 24, No. 5, pp. 852-864.
- Barton, N., K. Bakhtar, and S. Bandis. 1983. "Rock Joint Description and Modeling for Prediction of Near-Field Repository Performance," Materials Res. Soc. Ann. Meeting 1983. Boston, MA, Proc. Symp. D - "Scientific Basis for Nuclear Waste Management."
- Bixler, N. E. and R. R. Eaton. In preparation. "Sensitivity of Calculated Hydrologic Flows Through Multilayered Hard Rock to Computational Solution Procedures," Proceedings of DOE/NRC Symposium on Groundwater Flow and Transport Modeling, May 20-21, 1985, Albuquerque, NM.
- Brooks, R. H., and A. T. Corey. 1966. "Properties of Porous Media Affecting Fluid Flow," J. of the Irrig. and Drainage Div., Proceedings of the Amer. Soc. of Civil Engrs., IR2, pp. 61-88.
- Burdine, N. T. 1953. "Relative Permeability Calculations From Pore Size Distribution Data," Petroleum Transactions, AIME, T.P. 3519, Vol. 198, pp. 71-78.
- Campbell, J. E., D. E. Longsine, and R. M. Cranwell. 1981. "Risk Methodology for Geologic Disposal of Radioactive Waste: The NWFT/DVM Computer Code Users Manual," NUREG/CR-2081 (SAND81-0886), Sandia National Laboratories, Albuquerque, NM.
- DOE. 1984. "Draft Environmental Assessment - Yucca Mountain Site, Nevada Research and Development Area, Nevada," U.S. Department of Energy, Washington, D.C.
- Dudley, A. L., R. R. Peters, M. S. Tierney, E. A. Klavetter, J. H. Gauthier, and M. Wilson. In preparation. "Total Systems Performance Assessment Code (TOSPAC) Volume 1: Physical and Mathematical Bases," SAND85-0002, Sandia National Laboratories, Albuquerque, NM.
- Duguid, J., and P. C. Y. Lee. 1973. "Flow in Fractured Porous Media," Research Report No. 73-WR-1, Dept. of Civil and Geological Engineering, Princeton University, Princeton, NJ.
- Eaton, R. R., D. K. Gartling, and D. E. Larson. 1983. "SAGUARO - A Finite Element Computer Program for Partially Saturated Porous Flow Problems," SAND82-2772, Sandia National Laboratories, Albuquerque, NM.

- Froment, G. F., and K. B. Bischoff. 1979. "CHEMICAL REACTOR ANALYSIS AND DESIGN," John Wiley and Sons, New York, NY.
- Freeze, R. A., and J. A. Cherry. 1979. "GROUNDWATER," Prentice-Hall, Inc., Englewood Cliffs, NJ.
- Gringarten, A. C., and H. J. Ramey, Jr. 1974. "Unsteady-State Pressure Distribution Created With a Single Horizontal Fracture, Partial Penetration or Restricted Entry," Soc. Pet. Enj. J., Aug. pp. 413-426.
- Haverkamp, R., M. Vauclin, J. Touma, P. Wierenga, and G. Vachaud. 1977. "A Comparison of Numerical Simulation Models for One-Dimensional Infiltration," Soil Sci. Am. J., Vol 41, pp. 285-294.
- Hillel, D. 1982. "INTRODUCTION TO SOIL PHYSICS," Academic Press, New York, NY.
- Intera Environmental Consultants Inc. 1982. "NETFLO - A Network Ground-Water Flow Code," ONWI/E512-02900/CD-01, Houston, TX.
- Johnson, E. F., D. P. Bossler, and V. O. Naumann. 1959. "Calculation of Relative Permeability From Displacement Experiments," Petroleum Trans., 216, pp. 370-372.
- Klavetter, E. A., and R. R. Peters. 1985. "Estimation of Hydrologic Properties for an Unsaturated, Fractured Rock Mass," SAND84-2642, Sandia National Laboratories, Albuquerque, NM.
- Klavetter, E. A., R. R. Peters, and B. M. Schwartz. 1985. "Experimental Plan for Investigating Water Movement Through Fractures," SAND84-0468, Sandia National Laboratories, Albuquerque, NM.
- Martinez, M. J. In preparation. "Capillary Driven Flow in a Fracture Located in a Porous Media," SAND84-1697, Sandia National Laboratories, Albuquerque, NM.
- McTigue, D. F., R. K. Wilson, and J. W. Nunziato. 1984. "An Effective Stress Principle for Partially Saturated Media," SAND82-1977, Sandia National Laboratories, Albuquerque, NM.
- Montazer, P. and W. E. Wilson. 1984. "Conceptual Hydrologic Model of Flow in the Unsaturated Zone, Yucca Mountain, Nevada," Water-Resources Investigations Report 84-4345, U.S. Geological Survey, Denver, CO.
- Mualem, Y. 1976. "A New Model for Predicting the Hydraulic Conductivity of Unsaturated Porous Materials," Water Resources Research 12(3), pp. 513-522.
- Narasimhan, T. N. 1982. "Physics of Saturated-Unsaturated Subsurface Flow" in "Recent Trends in Hydrogeology" edited by T. N. Narasimhan, Special Paper 189, Geological Society of America, Boulder, CO.

- Nimick, F. B., S. J. Bauer, and J. R. Tillerson. 1984. "Recommended Matrix and Rock-Matrix Bulk, Mechanical and Thermal Properties for Thermomechanical Stratigraphy of Yucca Mountain," Keystone Doc. 6310-85-1, Sandia National Laboratories, Albuquerque, NM.
- Odeh, A. S., 1965. "Unsteady Behavior of Mutually Fractured Reservoirs," Soc. Pet. Enj. J., Vol. 5, pp. 60-65.
- Ortiz, T. S., R. L. Williams, F. B. Nimick, B. C. Whittet, and D. L. South. 1985. "A Three-Dimensional Model of the Thermal-Mechanical Units at Yucca Mountain, Southern Nevada," SAND84-1076, Sandia National Laboratories, Albuquerque, NM.
- Peters, R. R., E. A. Klavetter, I. J. Hall, S. C. Blair, P. R. Heller, and G. W. Gee. 1984. "Fracture and Matrix Hydrologic Characteristics of Tuffaceous Materials from Yucca Mountain, Nye County, Nevada," SAND84-1471, Sandia National Laboratories, Albuquerque, NM.
- Reeves, M., and J. O. Duguid. 1975. "Water Movement Through Saturated-Unsaturated Porous Media: A Finite-Element Galerkin Model," ORNL-4927, Oak Ridge National Laboratory, Oak Ridge, TN.
- Reisenauer, A. E., K. T. Key, T. N. Narasimhan, and R. W. Nelson. 1982. "TRUST: A Computer Program for Variably Saturated Flow in Multidimensional, Deformable Media," NUREG/CR-2360, U.S. Nuclear Regulatory Commission, Washington, D.C.
- Richards, L. A. 1931. "Capillary Conduction of Liquids Through Porous Mediums," [sic], Physics, Vol. 1, pp. 318-333.
- Rose, W. 1949. "Theoretical Generalizations Leading to the Evaluation of Relative Permeability," Petroleum Transactions, AIME, T.P. 2563, pp. 111-126.
- Scott, R. B., R. W. Spengler, A. R. Lappin, and M. P. Chornack. 1983. "Geologic Character of Tuffs in the Unsaturated Zone at Yucca Mountain, Southern Nevada," in "Role of the Unsaturated Zone in Radioactive and Hazardous Waste Disposal," edited by J. Mercer, Ann Arbor Science, Ann Arbor, MI.
- Sharp, J. C. 1970. "Fluid Flow Through Fissured Media," Ph.D. Thesis, Imp. Coll. of Sci. and Technol., London, England.
- Sinnock, S., Y. T. Lin, and J. P. Brannen. 1984. "Preliminary Bounds on the Expected Postclosure Performance of the Yucca Mountain Repository Site, Southern Nevada," SAND84-1492, Sandia National Laboratories, Albuquerque, NM.
- Snow, D. T. 1970. "The Frequency and Apertures of Fractures in Rock," Int. J. Rock Mech. Min. Sci., Vol. 7, pp. 23-40.

- Spengler, R. W. and M. P. Chornack. 1984. "Stratigraphic and Structural Characteristics of Volcanic Rocks in Core Hole USW G-4, Yucca Mountain, Nye County, Nevada," with a section on geophysical logs by D. C. Muller and J. Kibler; OFR 81-1349, U.S. Geological Survey, Denver, CO.
- Travis, B. J., S. W. Hodson, H. E. Nuttal, T. L. Cook, and R. S. Rundberg. 1984. "Preliminary Estimates of Water Flow and Radionuclide Transport in Yucca Mountain," Mat. Res. Soc. Symp. Proc., Vol. 26, pp. 1039-1047.
- van Genuchten, R. 1978. "Calculating the Unsaturated Hydraulic Conductivity With a New Closed Form Analytical Model," Water Resources Bulletin, Princeton University Press, Princeton University, Princeton, NJ.
- Wang, J. S. Y., and T. N. Narasimhan. 1985. "Hydrologic Mechanisms Governing Fluid Flow in Partially Saturated, Fractured, Porous Tuff at Yucca Mountain," SAND84-7202, Sandia National Laboratories, Albuquerque, NM.
- Warren, J. E., and P. J. Root. 1963. "Behavior of Naturally Fractured Reservoirs," Soc. Pet. Eng. J., Vol. 9, pp. 245-255.
- Wheeler, A. 1955. "CATALYSIS," Reinhold, New York, NY, edited by P. H. Emmett, Vol. 2, p. 105.

DISTRIBUTION LIST

B. C. Rusche (RW-1)  
Director  
Office of Civilian Radioactive  
Waste Management  
U.S. Department of Energy  
Forrestal Building  
Washington, DC 20585

Ralph Stein (RW-23)  
Office of Geologic Repositories  
U.S. Department of Energy  
Forrestal Building  
Washington, DC 20585

J. J. Fiore, (RW-22)  
Program Management Division  
Office of Geologic Repositories  
U.S. Department of Energy  
Forrestal Building  
Washington, DC 20585

M. W. Frei (RW-23)  
Engineering & Licensing Division  
Office of Geologic Repositories  
U.S. Department of Energy  
Forrestal Building  
Washington, DC 20585

E. S. Burton (RW-25)  
Siting Division  
Office of Geologic Repositories  
U.S. Department of Energy  
Forrestal Building  
Washington, D.C. 20585

C. R. Cooley (RW-24)  
Geosciences & Technology Division  
Office of Geologic Repositories  
U.S. Department of Energy  
Forrestal Building  
Washington, DC 20585

V. J. Cassella (RW-22)  
Office of Geologic Repositories  
U.S. Department of Energy  
Forrestal Building  
Washington, DC 20585

T. P. Longo (RW-25)  
Program Management Division  
Office of Geologic Repositories  
U.S. Department of Energy  
Forrestal Building  
Washington, DC 20585

Cy Klingsberg (RW-24)  
Geosciences and Technology Division  
Office of Geologic Repositories  
U. S. Department of Energy  
Forrestal Building  
Washington, DC 20585

B. G. Gale (RW-25)  
Siting Division  
Office of Geologic Repositories  
U.S. Department of Energy  
Forrestal Building  
Washington, D.C. 20585

R. J. Blaney (RW-22)  
Program Management Division  
Office of Geologic Repositories  
U.S. Department of Energy  
Forrestal Building  
Washington, DC 20585

R. W. Gale (RW-40)  
Office of Policy, Integration, and  
Outreach  
U.S. Department of Energy  
Forrestal Building  
Washington, D.C. 20585

J. E. Shaheen (RW-44)  
Outreach Programs  
Office of Policy, Integration and  
Outreach  
U.S. Department of Energy  
Forrestal Building  
Washington, DC 20585

J. O. Neff, Manager  
Salt Repository Project Office  
U.S. Department of Energy  
505 King Avenue  
Columbus, OH 43201

D. C. Newton (RW-23)  
Engineering & Licensing Division  
Office of Geologic Repositories  
U.S. Department of Energy  
Forrestal Building  
Washington, DC 20585

S. A. Mann, Manager  
Crystalline Rock Project Office  
U.S. Department of Energy  
9800 South Cass Avenue  
Argonne, IL 60439

O. L. Olson, Manager  
Basalt Waste Isolation Project Office  
U.S. Department of Energy  
Richland Operations Office  
Post Office Box 550  
Richland, WA 99352

K. Street, Jr.  
Lawrence Livermore National  
Laboratory  
Post Office Box 808  
Mail Stop L-209  
Livermore, CA 94550

D. L. Vieth, Director (4)  
Waste Management Project Office  
U.S. Department of Energy  
Post Office Box 14100  
Las Vegas, NV 89114

L. D. Ramspott (3)  
Technical Project Officer for NNWSI  
Lawrence Livermore National  
Laboratory  
P.O. Box 808  
Mail Stop L-204  
Livermore, CA 94550

D. F. Miller, Director  
Office of Public Affairs  
U.S. Department of Energy  
Post Office Box 14100  
Las Vegas, NV 89114

W. J. Purcell (RW-20)  
Office of Geologic Repositories  
U.S. Department of Energy  
Forrestal Building  
Washington, DC 20585

D. A. Nowack (12)  
Office of Public Affairs  
U.S. Department of Energy  
Post Office Box 14100  
Las Vegas, NV 89114

D. T. Oakley (4)  
Technical Project Officer for NNWSI  
Los Alamos National Laboratory  
P.O. Box 1663  
Mail Stop F-619  
Los Alamos, NM 87545

B. W. Church, Director  
Health Physics Division  
U.S. Department of Energy  
Post Office Box 14100  
Las Vegas, NV 89114

W. W. Dudley, Jr. (3)  
Technical Project Officer for NNWSI  
U.S. Geological Survey  
Post Office Box 25046  
418 Federal Center  
Denver, CO 80225

Chief, Repository Projects Branch  
Division of Waste Management  
U.S. Nuclear Regulatory Commission  
Washington, D.C. 20555

NTS Section Leader  
Repository Project Branch  
Division of Waste Management  
U.S. Nuclear Regulatory Commission  
Washington, D.C. 20555

Document Control Center  
Division of Waste Management  
U.S. Nuclear Regulatory Commission  
Washington, D.C. 20555

V. M. Glanzman  
U.S. Geological Survey  
Post Office Box 25046  
913 Federal Center  
Denver, CO 80225

P. T. Prestholt  
NRC Site Representative  
1050 East Flamingo Road  
Suite 319  
Las Vegas, NV 89109

M. E. Spaeth  
Technical Project Officer for NNWSI  
Science Applications  
International, Corporation  
2769 South Highland Drive  
Las Vegas, NV 89109

SAIC-T&MSS Library (2)  
Science Applications  
International, Corporation  
2950 South Highland Drive  
Las Vegas, NV 89109

W. S. Twenhofel, Consultant  
Science Applications  
International, Corp.  
820 Estes Street  
Lakewood, CO 80215

A. E. Gurrola  
General Manager  
Energy Support Division  
Holmes & Narver, Inc.  
Post Office Box 14340  
Las Vegas, NV 89114

J. A. Cross, Manager  
Las Vegas Branch  
Fenix & Scisson, Inc.  
Post Office Box 15408  
Las Vegas, NV 89114

Neal Duncan (RW-44)  
Office of Policy, Integration, and  
Outreach  
U.S. Department of Energy  
Forrestal Building  
Washington, DC 20585

J. S. Wright  
Technical Project Officer for NNWSI  
Westinghouse Electric Corporation  
Waste Technology Services Division  
Nevada Operations  
Post Office Box 708  
Mail Stop 703  
Mercury, NV 89023

ONWI Library  
Battelle Columbus Laboratory  
Office of Nuclear Waste Isolation  
505 King Avenue  
Columbus, OH 43201

W. M. Hewitt, Program Manager  
Roy F. Weston, Inc.  
2301 Research Blvd., 3rd Floor  
Rockville, MD 20850

H. D. Cunningham  
General Manager  
Reynolds Electrical &  
Engineering Co., Inc.  
Post Office Box 14400  
Mail Stop 555  
Las Vegas, NV 89114

T. Hay, Executive Assistant  
Office of the Governor  
State of Nevada  
Capitol Complex  
Carson City, NV 89710

R. R. Loux, Jr., Director (3)  
Nuclear Waste Project Office  
State of Nevada  
Capitol Complex  
Carson City, NV 89710

C. H. Johnson, Technical  
Program Manager  
Nuclear Waste Project Office  
State of Nevada  
Capitol Complex  
Carson City, NV 89710

John Fordham  
Desert Research Institute  
Water Resources Center  
Post Office Box 60220  
Reno, NV 89506

Department of Comprehensive  
Planning  
Clark County  
225 Bridger Avenue, 7th Floor  
Las Vegas, NV 89155

Lincoln County Commission  
Lincoln County  
Post Office Box 90  
Pioche, NV 89043

Community Planning and  
Development  
City of North Las Vegas  
Post Office Box 4086  
North Las Vegas, NV 89030

City Manager  
City of Henderson  
Henderson, NV 89015

N. A. Norman  
Project Manager  
Bechtel National Inc.  
P. O. Box 3965  
San Francisco, CA 94119

Flo Butler  
Los Alamos Technical Associates  
1650 Trinity Drive  
Los Alamos, New Mexico 87544

Timothy G. Barbour  
Science Applications  
International Corporation  
1626 Cole Boulevard, Suite 270  
Golden, CO 80401

Dr. Martin Mifflin  
Desert Research Institute  
Water Resources Center  
Suite 1  
2505 Chandler Avenue  
Las Vegas, NV 89120

Planning Department  
Nye County  
Post Office Box 153  
Tonopah, NV 89049

Economic Development  
Department  
City of Las Vegas  
400 East Stewart Avenue  
Las Vegas, NV 89101

Director of Community  
Planning  
City of Boulder City  
Post Office Box 367  
Boulder City, NV 89005

Commission of the  
European Communities  
200 Rue de la Loi  
B-1049 Brussels  
BELGIUM

Technical Information Center  
Roy F. Weston, Inc.  
2301 Research Boulevard,  
Third Floor  
Rockville, MD 20850

R. Harig  
Parsons Brinkerhoff Quade &  
Douglas, Inc.  
1625 Van Ness Ave.  
San Francisco, CA 94109-3678

Dr. Madan M. Singh, President  
Engineers International, Inc.  
98 East Naperville Road  
Westmont, IL 60559-1595

E. P. Binnall  
Field Systems Group Leader  
Building 50B/4235  
Lawrence Berkeley Laboratory  
Berkeley, CA 94720

J. E. Gale  
Groundwater Research Inst.  
Dept. of Earth Sciences  
U. of Waterloo  
Waterloo, Ontario  
Canada  
N2L 3G1

D. Hodgkinson  
Theoretical Physics Div.  
AERE Harwell  
Oxfordshire OX11 0RA  
United Kingdom

R. B. Lyon  
Acting Dir., Nuclear Fuel  
Waste Management  
Atomic Energy of Canada, Ltd.  
Pinawa, Manitoba ROE 1LO  
Canada

P. Raimbault  
CEA/PSH  
SAED/SASICC-DAS  
CEN FAR BP.6  
92260 Fonteney aux Roses  
France

R. Codell  
U.S. NRC  
Washington, D.C. 20555

G. Dagen  
Dept. of Mech. and Env.  
Engineering  
U. of California  
Santa Barbara, CA 93106

F. H. Dove  
Pacific Northwest Laboratory  
P. O. Box 999  
Richland, WA 99352

Roger Hart  
Itasca Consulting Group, Inc.  
P.O. Box 14806  
Minneapolis, Minnesota 55414

A. Herbert  
AERE Harwell  
Oxfordshire OX11 0RA  
United Kingdom

A. Larsson  
Swedish Nuclear Power Inspectorate  
Box 27106  
S-102 52 Stockholm, Sweden

I. Neretnieks  
Dept. Chemical Engineering  
Royal Institute of Technology  
S-10044 Stockholm, Sweden

D. Alexander  
RW24 OCRWM  
7F088 Forrestal Building  
Washington, D.C. 20585

C. Cole  
Pacific Northwest Laboratory  
P.O. Box 999  
Richland, WA 99352

S. Davis  
Dept. of Hydrology and Water Res.  
U. of Arizona  
Tucson, AZ 85719

K. Eggert  
Lawrence Livermore Nat.  
Laboratories  
P. O. Box 808 L206  
Livermore, CA 94550

D. Evans  
Dept. of Hydrology and Water Res.  
U. of Arizona  
Tucson, AZ 85719

D.R.F. Harleman  
Ford Professor of Engineering  
Massachusetts Institute of  
Technology  
Cambridge, MA 02139

S. Key  
Re/Spec Inc.  
Box 1984  
3515 Eubank NE  
Albuquerque, NM 87191

P. Montazer  
USGS-WRD, Mail Stop 416  
Federal Center  
Denver, CO 80225

S. Neuman  
Dept. of Hydrology and Water Res.  
U. of Arizona  
Tucson, AZ 85719

W.W. Owens  
6269 S. Knoxville  
Tulsa, OK 74136

G. Pinder  
Princeton University  
Civil Engineering Dept.  
Princeton, NJ

B. Ross  
Disposal Safety Inc.  
1211 Conn. Ave. NW  
Suite 610  
Washington, D.C. 20036

D. Stevens  
Dept. of Soil Sciences  
NM. Tech.  
Socorro, NM 87801

D. T. Hoxie  
U.S. Geological Survey  
MS 416, Box 25046  
Denver Federal Center  
Denver, CO 80225

G. W. Gee  
Pacific Northwest Laboratory  
P.O. Box 999  
Richland, WA 99352

P. Kelsall  
IT Corporation  
2340 S. Alamo  
Albuquerque, NM 87106

J. A. Lieberman  
OTHA, Inc.  
P. O. Box 651  
Glen Echo, MD 20812

T. N. Narasimhan  
Lawrence Berkeley Laboratories  
U. of California  
Berkeley, CA 94720

T. J. Nicholson  
Earth Sci. Branch  
USNRC Mail Stop 1130-55  
Washington, D.C. 20815

T. R. Pigford  
Dept of Nuclear Engineering  
U. of California  
Berkeley, CA 94720

K. Pruess  
Lawrence Berkeley Laboratories  
Berkeley, CA 97420

J. Rulon  
Lawrence Berkeley Laboratories  
Berkeley, CA 97420

M. Teubner  
Science Applications International  
Corporation  
Valley Bank Center  
101 Convention Center Dr.  
Suite 407  
Las Vegas, NV 89109

B. J. Travis  
Los Alamos Nat. Laboratory  
P. O. Box 1663  
Los Alamos, NM 87545

S. Tyler  
DRI  
2505 Chandler Ave., Suite 1  
Las Vegas, NV 89120

J. S. Y. Wang  
Earth Science Division  
Lawrence Berkeley Laboratories  
Berkeley, CA 97420

W. E. Wilson  
USGS-WRD, Mail Stop 416  
Federal Center  
Denver, CO 80225

D. T. Hoxie  
U.S. Geological Survey  
MS 416, Box 25046  
Denver Federal Center  
Denver, CO 80225

G. S. Bodvarsson  
Lawrence Berkeley Laboratory  
Berkeley, CA 97420

1511 N. E. Bixler  
1511 R. R. Eaton  
6300 R. W. Lynch  
6310 T. O. Hunter  
6310 CF 72-12144-1.6/NQ  
6311 L. W. Scully  
6311 C. Mora  
6312 G. E. Barr  
6312 F. W. Bingham  
6312 A. L. Dudley  
6312 J. H. Gauthier  
6312 N. K. Hayden  
6312 B. S. Langkopf  
6312 R. R. Peters (20)  
6312 R. W. Prindle  
6312 M. S. Tierney  
6312 M. Wilson  
6312 J. G. Yeager  
6313 T. E. Blejwas  
6313 E. A. Klavetter (20)  
6313 F. B. Nimick  
6313 R. M. Zimmerman  
6314 J. A. Fernandez  
6314 J. R. Tillerson  
6315 Y. T. Lin  
6315 S. Sinnock  
6331 A. R. Lappin  
6332 WMT Library (20)  
6430 N. R. Ortiz  
6431 E. J. Bonano  
6431 R. M. Cranwell  
6431 R. Guzowski  
7223 R. G. Easterling  
7223 F. W. Spencer  
7223 I. J. Hall  
3141 S. A. Landenberger (5)  
3151 W. L. Garner (3)  
8024 P. W. Dean  
3154-3 C. H. Dalin (28)  
for DOE/OSTI